Article

Molecular Cell

Dinucleotide Degradation by REXO2 Maintains Promoter Specificity in Mammalian Mitochondria

Graphical Abstract

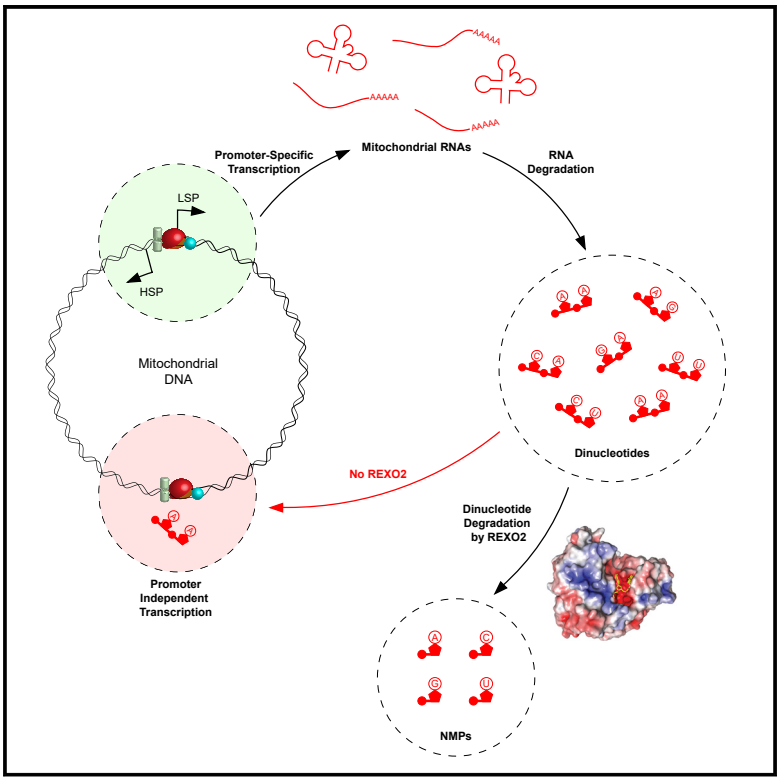

Highlights

- REXO2 is a specialized dinucleotidase present in mammalian mitochondria
- REXO2 is essential for embryonic development in mice
- Dinucleotides stimulate mitochondrial transcription *in vitro* and *in vivo*
- Dinucleotide degradation is required to prevent their use as transcription primers

Authors

Thomas J. Nicholls, Henrik Spåhr, Shan Jiang, ..., Aleksandra Filipovska, Nils-Göran Larsson, Claes M. Gustafsson

Correspondence

nils-goran.larsson@ki.se (N.-G.L.), claes.gustafsson@medkem.gu.se (C.M.G.)

In Brief

Nicholls et al. study the function of the human oligoribonuclease REXO2 and find that it is a specialized dinucleotidase. The *Rexo2* gene is essential for embryonic development, and its conditional loss results in changes to mitochondrial transcription patterns, indicating the use of dinucleotides for promoter-independent mitochondrial transcription initiation.

Nicholls et al., 2019, Molecular Cell *76*, 1–13
December 5, 2019
https://doi.org/10.1016/j.molcel.2019.09.010

CellPress

Please cite this article in press as: Nicholls et al., Dinucleotide Degradation by REXO2 Maintains Promoter Specificity in Mammalian Mitochondria, Molecular Cell (2019), https://doi.org/10.1016/j.molcel.2019.09.010

Molecular Cell
Article

Dinucleotide Degradation by REXO2 Maintains Promoter Specificity in Mammalian Mitochondria

Thomas J. Nicholls,[1,12,14] Henrik Spåhr,[2,3,4,14] Shan Jiang,[3,4] Stefan J. Siira,[5,6] Camilla Koolmeister,[3,4] Sushma Sharma,[7] Johanna H.K. Kauppila,[2] Min Jiang,[2,13] Volkhard Kaever,[8] Oliver Rackham,[5,9,10] Andrei Chabes,[7] Maria Falkenberg,[1] Aleksandra Filipovska,[5,11] Nils-Göran Larsson,[3,4,*] and Claes M. Gustafsson[1,15,*]

[1]Department of Medical Biochemistry and Cell Biology, University of Gothenburg, PO Box 440, Gothenburg 405 30, Sweden
[2]Department of Mitochondrial Biology, Max Planck Institute for Biology of Ageing, 50931 Cologne, Germany
[3]Department of Medical Biochemistry and Biophysics, Karolinska Institutet, Stockholm 17177, Sweden
[4]Max Planck Institute for Biology of Ageing - Karolinska Institutet Laboratory, Karolinska Institutet, Stockholm 17177, Sweden
[5]Harry Perkins Institute of Medical Research, Nedlands, WA 6009, Australia
[6]Centre for Medical Research, The University of Western Australia, Nedlands, WA 6009, Australia
[7]Department of Medical Biochemistry and Biophysics, Umeå University, Umeå 901 87, Sweden
[8]Research Core Unit Metabolomics, Hannover Medical School, 30625 Hannover, Germany
[9]School of Pharmacy and Biomedical Sciences, Curtin University, Bentley, WA 6102, Australia
[10]Curtin Health Innovation Research Institute, Curtin University, Bentley, WA 6102, Australia
[11]School of Molecular Sciences, The University of Western Australia, Nedlands, WA, Australia
[12]Present address: Wellcome Centre for Mitochondrial Research, Institute for Cell and Molecular Biosciences, The Medical School, Newcastle University, Newcastle upon Tyne, NE2 4HH, UK
[13]Present address: School of Life Sciences, Westlake University, Hangzhou, China
[14]These authors contributed equally
[15]Lead Contact
*Correspondence: nils-goran.larsson@ki.se (N.-G.L.), claes.gustafsson@medkem.gu.se (C.M.G.)
https://doi.org/10.1016/j.molcel.2019.09.010

SUMMARY

Oligoribonucleases are conserved enzymes that degrade short RNA molecules of up to 5 nt in length and are assumed to constitute the final stage of RNA turnover. Here we demonstrate that REXO2 is a specialized dinucleotide-degrading enzyme that shows no preference between RNA and DNA dinucleotide substrates. A heart- and skeletal-muscle-specific knockout mouse displays elevated dinucleotide levels and alterations in gene expression patterns indicative of aberrant dinucleotide-primed transcription initiation. We find that dinucleotides act as potent stimulators of mitochondrial transcription initiation *in vitro*. Our data demonstrate that increased levels of dinucleotides can be used to initiate transcription, leading to an increase in transcription levels from both mitochondrial promoters and other, nonspecific sequence elements in mitochondrial DNA. Efficient RNA turnover by REXO2 is thus required to maintain promoter specificity and proper regulation of transcription in mammalian mitochondria.

INTRODUCTION

The mammalian mitochondrial genome encodes 13 essential protein components of the mitochondrial oxidative phosphorylation system, as well as the full complement of tRNAs and rRNAs required for the synthesis of these proteins within mitochondria. The life cycle of a mitochondrial RNA (mtRNA) molecule begins with transcription initiation from one of two promoters, the light-strand promoter (LSP) or the heavy-strand promoter (HSP) (Gustafsson et al., 2016). Transcription initiation minimally requires three proteins comprising a bacteriophage T7-like mtRNA polymerase (POLRMT) together with mitochondrial transcription factor A (TFAM) and transcription factor B2 (TFB2M) (Falkenberg et al., 2002; Shi et al., 2012). A stepwise model for mitochondrial transcription initiation has been elucidated from biochemical and structural studies in recent years. First, TFAM binds to the promoter region, imposing a sharp U-turn in the DNA and recruiting POLRMT, which becomes positioned at the transcription start site (TSS) (Gaspari et al., 2004; Morozov et al., 2014). TFB2M then binds to this complex and facilitates melting of the promoter DNA (Hillen et al., 2017; Morozov et al., 2015; Posse and Gustafsson, 2017; Sologub et al., 2009), allowing POLRMT to initiate RNA synthesis.

Transcription in mitochondria is polycistronic, with mRNAs and rRNAs interspersed ("punctuated") with tRNAs (Ojala et al., 1981). Once these tRNAs have folded into their canonical cloverleaf structures in the precursor RNAs, they are recognized and cleaved at their 5′ and 3′ ends by RNase P and ELAC2, respectively (Brzezniak et al., 2011; Holzmann et al., 2008; Sanchez et al., 2011), which serve to excise individual transcripts.

The degradation of mtRNAs has long been poorly understood but has seen several recent advances. The most well-characterized degradation machinery in the human mitochondrial matrix is a complex of the phosphorylytic exoribonuclease PNPase with the helicase SUV3, collectively termed the RNA degradosome (Borowski et al., 2013; Szczesny et al., 2010). PNPase processively releases mononucleoside diphosphates as reaction products but is unable to degrade short RNA molecules of less than

~4 nt in length (Lin et al., 2012). The loss of mitochondrial PNPase causes the accumulation of antisense RNAs (Pietras et al., 2018) as well as double-stranded RNAs (Dhir et al., 2018), implicating a role for PNPase in the removal of these molecules, and it remains unclear which other RNases also contribute to RNA turnover.

In *E. coli*, the final stage of RNA degradation is the hydrolysis of short RNA fragments of 2–5 nt in length, termed nanoRNAs (Mechold et al., 2007). This process requires the conserved and essential oligoribonuclease Orn (Ghosh and Deutscher, 1999; Niyogi and Datta, 1975). Orn is a 3′-5′ exonuclease of the DEDDh family that releases mononucleotides as reaction products (Datta and Niyogi, 1975) and was recently found to show a strong preference for dinucleotide substrates (Kim et al., 2019). The loss of Orn results in large-scale alterations in gene expression that have been attributed to the ability of nanoRNAs to mediate transcription priming (Druzhinin et al., 2015; Goldman et al., 2011; Vvedenskaya et al., 2012).

The human homolog of Orn is called REXO2 and is an active ribonuclease (Mechold et al., 2006; Nguyen et al., 2000) that localizes to the mitochondrial matrix, the intermembrane space, and the cytosol (Bruni et al., 2013). Depletion of REXO2 in human cells causes severe effects on mitochondrial DNA copy number, mitochondrial transcript levels, and mitochondrial translation (Bruni et al., 2013), but the molecular basis for these wide-ranging effects on mitochondrial gene expression are unclear.

In this work, we reassess the role of REXO2 in mitochondria. We find that REXO2 is a sugar-independent dinucleotide-degrading enzyme, as supported by *in vitro* biochemistry and crystal structures of the apo and substrate-bound enzyme forms. We find that REXO2 is an essential gene in mice and that a heart- and skeletal-muscle-specific conditional knockout model exhibits changes in both promoter-dependent and promoter-independent transcription initiation indicating dinucleotide-mediated priming of mitochondrial transcription from both canonical and non-canonical sites.

Therefore we conclude that the activity of REXO2 is essential for both RNA turnover and the maintenance of promoter specificity in mammalian mitochondria.

RESULTS

REXO2 Is an RNA and DNA Dinucleotidase

REXO2 degrades oligonucleotides of ~5 nt in length, with a preference for RNA substrates (Chu et al., 2019; Nguyen et al., 2000). We expressed and purified full-length human REXO2 from *E. coli* (Figure S1A) and assessed the activity of the recombinant protein upon nanoRNA substrates *in vitro*. REXO2 exhibited a strong preference for dinucleotides relative to 3-, 4-, or 5-mer substrates, with little sequence specificity (Figures 1A and 1B). RNA 3-, 4-, or 5-mers could be fully degraded only at significantly higher enzyme concentrations (Figures S1B and S1D). Surprisingly, when the activity of recombinant REXO2 was assessed upon DNA oligonucleotides of equivalent sequences, a comparable activity was observed as the one obtained with RNA dinucleotides (Figures 1C and 1D). However, no activity was observed upon longer DNA oligos of 3–5 nt in length at these enzyme concentrations (Figures 1C and 1D) or even at higher concentrations (Figures S1C and S1E), demonstrating that this sugar-nonspecific activity of REXO2 is restricted to dinucleotide substrates.

Structural Basis for REXO2 Substrate Specificity

To gain molecular insight into the mechanism and specificity of nucleotide degradation by REXO2, we crystallized the human protein comprising residues 39–216, which retains catalytic activity (Figures S1F–S1I), and determined its structure to 2.0 Å resolution (Table 1). As previously reported (Chu et al., 2019; Kim et al., 2019), the protein crystallizes as a dimer and has an RNase-H-like fold that is composed of five central β strands surrounded by nine α helices on opposite sides (Figures 2A and S2C). Each monomer harbors an active site formed by the conserved acidic DEDD residues D47, E49, D147, and D199 that are positioned for nucleotide binding (Figure 2A), and mutation of any one of the conserved DEDD residues to alanine severely impaired the catalytic activity of the enzyme (Figures 2B–2D), consistent with their key role in catalysis.

In order to understand the structural basis of the observed substrate specificity, we determined the structure of REXO2 complexed with either an RNA dinucleotide (pApA) or DNA dinucleotide (dAdA) in an arrested pre-catalytic state by mutating one of the DEDDh residues, D199A (Figures 2E–2G, S3B, and S3C; Table 1). The binding of dinucleotides produced only a few significant changes in the protein structure, mainly confined to a "trigger loop" between α9 and α10 of monomer A. This contains H194, which makes a 180° shift toward the active site to bind Zn^{2+} and the phosphate oxygen OP1 of the 3′ nucleotide. This structural arrangement is in stark contrast to the apoprotein, in which the DEDDh residue H194 faces away from the active site (Figures 2A and S3A). On the 5′ end of the dinucleotide, S143 and S170 of monomer A and R165 of monomer B form hydrogen bonds with OP1 of the nucleotide monophosphate, creating a physical boundary of the narrow active site that impedes binding of longer substrates (Figure 2G). Indeed, a structural comparison to other DEDD exonucleases (Figures S3D–S3F; Table S1) confirmed that a steric clash would be imposed starting from the third nucleotide, with additional clashes from nucleotide four and beyond, providing the structural basis for the strong preference of REXO2 for dinucleotide substrates.

The REXO2 dimer forms an extensive binding interface that corresponds to 16% of the surface area of each monomer (Figures 3A and S3G). To validate the functional importance of dimerization, we created amino acid substitutions designed to break this interface (Figures 3A, 3B, and S3H–S3K) and found that mutations that disrupt dimerization (Figure 3C) lead to a loss of enzymatic activity (Figure 3D).

REXO2 Is Essential for Embryonic Development

To investigate the *in vivo* importance for REXO2's ability to degrade dinucleotides, we generated a *Rexo2* conditional knockout allele ($Rexo2^{+/loxP}$) using the Cre-*loxP* system. Heterozygous knockout mice ($Rexo2^{+/-}$) were obtained by breeding $Rexo2^{+/loxP}$ mice with transgenic mice expressing Cre recombinase (+/*β-actin-cre*) (Figure S4A). Intercrossing of $Rexo2^{+/-}$ mice produced no viable homozygous knockout ($Rexo2^{-/-}$) mice (analyzed offspring, n = 119; $Rexo2^{+/+}$,

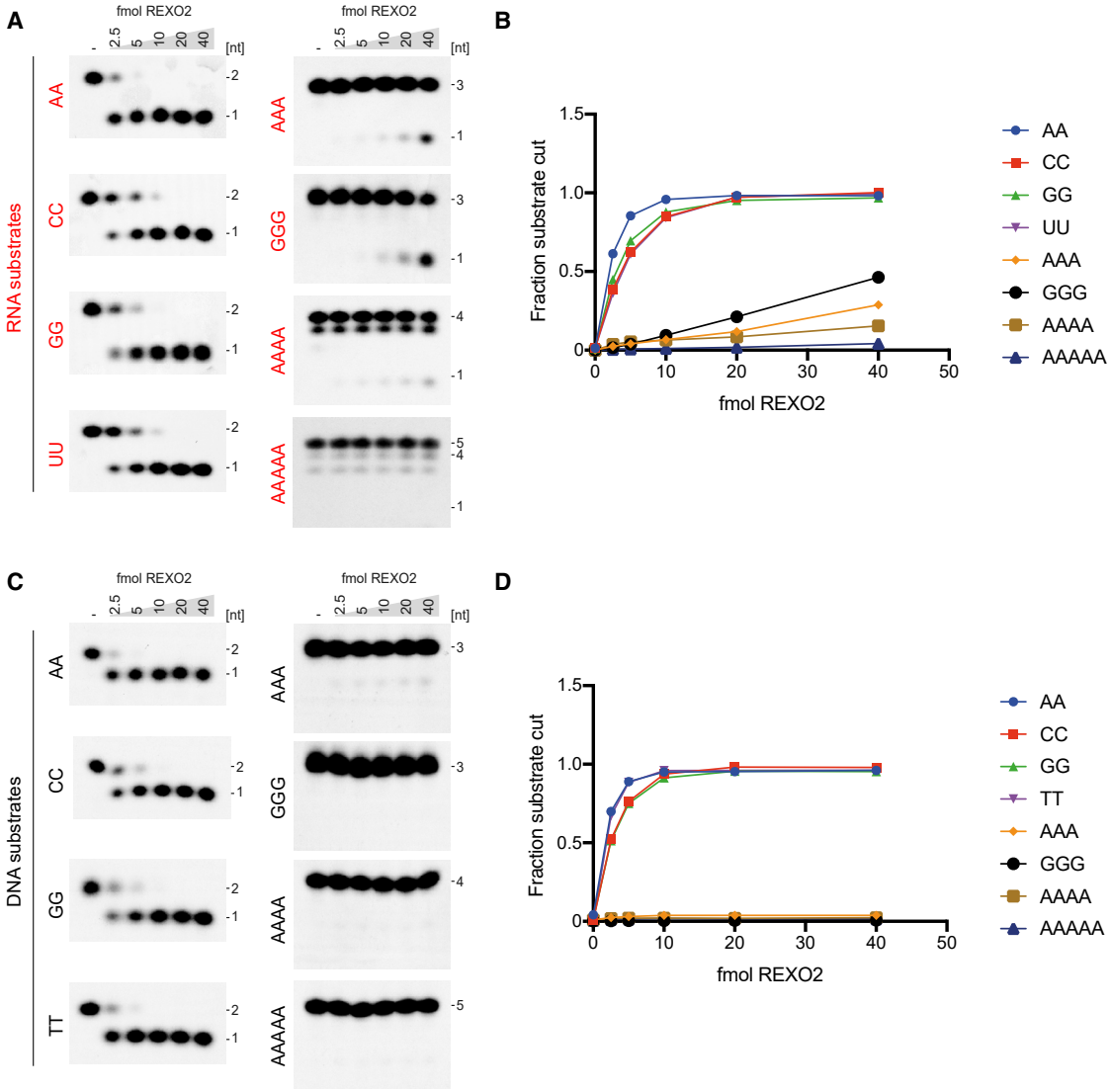

Figure 1. Human REXO2 Is a Dinucleotidase

(A) Activity of wild-type REXO2 upon RNA substrates of different lengths. Monophosphorylated radiolabeled substrate (10 fmol) was incubated with the indicated amount of REXO2 at 37°C for 30 min, separated by 18% urea-PAGE, and imaged by autoradiography.

(B) Quantification of RNA degradation by REXO2 from (A).

(C) Activity of wild-type REXO2 upon DNA substrates of different lengths. Monophosphorylated radiolabeled substrate (10 fmol) was incubated with the indicated amount of REXO2 at 37°C for 30 min, separated by 18% urea-PAGE, and imaged by autoradiography.

(D) Quantification of DNA degradation by REXO2 from (C).

n = 48; *Rexo2*$^{+/-}$, n = 71; and *Rexo2*$^{-/-}$, n = 0), indicating that loss of *Rexo2* results in embryonic lethality. Next, we performed an intercross of *Rexo2*$^{+/-}$ mice and analyzed embryos at embryonic day 8.5 (E8.5; analyzed embryos, n = 13). Embryos with the *Rexo2*$^{+/+}$ (n = 3) or *Rexo2*$^{+/-}$ (n = 8) genotype were well developed with normal appearance (Figure 4A), while embryos with the *Rexo2*$^{-/-}$ genotype (n = 2) were small and lacked heart structure (Figure 4B). Thus, *Rexo2* is essential for embryonic development, and loss of REXO2 causes embryonic lethality before E8.5.

We next disrupted *Rexo2* in heart and skeletal muscle by breeding *Rexo2*$^{+/loxP}$ mice with transgenic mice expressing Cre recombinase from the muscle creatinine kinase promoter (*Ckmm-cre*). The conditional knockout *Rexo2* mice (*Rexo2*$^{loxP/loxP}$, +/*Ckmm-cre*), hereafter denoted L/L, cre, were born at expected Mendelian ratios. Loss of REXO2 in heart was verified using western blotting (Figure 4C) and qPCR analyses (Figure S4B). The loss of REXO2 in heart and skeletal muscle did not lead to any obvious phenotype, and all mice were viable and healthy at the age of 52 weeks. No differences were observed between control and *Rexo2* knockout mice in body weight (Figure S4C), heart weight (Figure S4D), or mtDNA copy number (Figure 4D). We used northern blotting to analyze the effects of REXO2 loss on steady-state levels of

Table 1. Data Collection and Refinement Statistics

	REXO2	REXO2-D199A-pApA	REXO2-D199A-dAdA
Data Collection			
Wavelength (Å)	0.9184	0.9762	1.2824
Space group	$C222_1$	$C222_1$	$C222_1$
Cell dimensions			
a, *b*, *c* (Å)	36.2, 128.5, 170.2	35.6, 125.8, 167.9	35.8, 126.9, 168.2
α, β, γ (°)	90, 90, 90	90, 90, 90	90, 90, 90
Resolution (Å)	42.6–2.0 (2.12-2.00)	42.0–2.0 (2.04-1.97)	42.1-2.25 (2.38-2.25)
R_{meas} (%)	10.8 (93.5)	8.0 (165.8)	7.7 (150.4)
$CC_{1/2}$	99.7 (56.4)	99.9 (69.9)	99.9 (53.6)
$I/\sigma(I)$	8.47 (1.26)	13.4 (1.1)	14.2 (1.2)
Completeness (%)	98.8 (97.8)	100.0 (100.0)	99.7 (98.6)
Refinement			
Resolution (Å)	22.7-2.00 (2.01-2.00)	41.98-1.97 (1.98-1.97)	21.8-2.25 (2.33-2.25)
No. reflections	27274	27319	18796
R_{work}/R_{free}	0.1978/ 0.2322	0.2029/ 0.2512	0.2121/ 0.2480
No. atoms			
Protein	2663	2675	2675
Nucleic acid		44	42
Water	247	197	83
B-factors			
Protein	48.97	58.33	73.27
Nucleic acid		57.00	71.63
Water	51.49	62.60	69.90
RMSDs			
Bond lengths (Å)	0.010	0.010	0.010
Bond angles (°)	1.59	1.58	1.58
Ramachandran plot favored/ allowed (%)[a]	99.37/0.63	99.06/0.94	99.38/0.62
Clashscore[a]	1.13	1.85	1.11
Molprobity score[a]	0.82	0.95	0.82

Statistics for the highest-resolution shell are shown in parentheses.[a]According to the definition used in Molprobity (Lovell et al., 2003).

mtRNAs and found that there were no significant differences in the levels of mitochondrial rRNAs (mt-rRNAs), mitochondrial mRNAs (mt-mRNAs), and mitochondrial tRNAs (mt-tRNAs) between Rexo2 knockout mice and controls (Figures 4E, 4F, S4E, and S4F). To determine whether mitochondrial dinucleotides are *in vivo* substrates of REXO2, we measured the abundance of the pApA RNA dinucleotide using liquid-chromatography-tandem mass spectrometry (LC-MS/MS). A marked increase in the level of RNA pApA was observed in both whole heart tissue (Figure 4G) and isolated mitochondria (Figure 4H) in the absence of REXO2, suggesting that this is a substrate of mitochondrial REXO2 *in vivo*.

Accumulation of Dinucleotides Results in Promoter-Independent Transcription Initiation

We used parallel analyses of RNA ends (PARE) to determine the distribution of 5′ ends across the entire mitochondrial transcriptome and reveal additional mitochondrial gene expression changes in the absence of REXO2. This method captures ~20-nt-long tags from the 5′ ends of 5′-monophosphorylated RNAs (Rackham et al., 2016), with the normalized read count at each 5′ terminal position appearing as a peak enabling the identification of 5′ sites from canonical, *de novo*, or degraded transcripts. We identified numerous non-canonical peaks that are enriched in the absence of REXO2 (Figure 5A, shown in red). To assess whether these changes may be attributed to alterations of ribonucleoside triphosphate (NTP) levels in the absence of REXO2, we measured nucleotide concentrations from either whole heart tissue or isolated mitochondria of wild-type and *Rexo2* knockout mice (Figures S5A and S5B), which did not reveal any significant differences. However, by analyzing the frequency of different dinucleotide sequences at the 5′ ends of captured sequence tags, we found that in *Rexo2* knockout mice, there was an enrichment of AA, AC, and AT dinucleotides, while all other 5′ dinucleotides were depleted (Figure 5B). As ATP is used as the initiating nucleotide at both promoters *in vivo* by the mtRNA polymerase, we reasoned that the accumulation of dinucleotides (Figures 4G–4H) upon loss of REXO2 may prime low levels of transcription at non-canonical sites.

To validate this finding, we used a reconstituted human mitochondrial *in vitro* transcription system consisting of POLRMT and the two essential transcription factors, TFAM and TFB2M (Falkenberg et al., 2002). Transcription initiation by this complex usually requires one of the two mtDNA promoters, LSP or HSP. Accordingly, no transcription initiation is observed using a plasmid template lacking a promoter sequence (Figure 5C, lane 3). However, upon the addition of oligonucleotide(A) nanoRNAs to this reaction, we observed robust transcription initiation in the absence of a recognizable promoter (Figure 5C, lanes 4–7). Transcription initiation without a promoter was only observed using RNA primers (Figure 5C, compare lanes 4–7 with lanes 8–11) and only with closed circular templates, not with linear templates (Figure 5D). This indicates that negative supercoiling of circular DNA molecules is required for nanoRNAs to access the template in order to prime transcription. The ability of nanoRNAs to prime transcription remained evident at low concentrations relative to that of the normal initiating nucleotide ATP (Figures S5C and S5D), indicating that nanoRNAs are potent primers of promoter-independent mitochondrial transcription. Furthermore, by using nanoRNAs of different sequences, we found that different nanoRNA sequences are capable of priming promoter nonspecific transcription providing that the 3′ end contains a pair of adenine residues (Figure S5E, lanes 10–14), highlighting their potential to exert broad effects upon transcription.

nanoRNAs Stimulate Promoter-Dependent Transcription Initiation

Next, we investigated the effects of the loss of REXO2 upon promoter-dependent transcription initiation from the two mtDNA promoters, LSP and HSP. The rate of transcription initiation

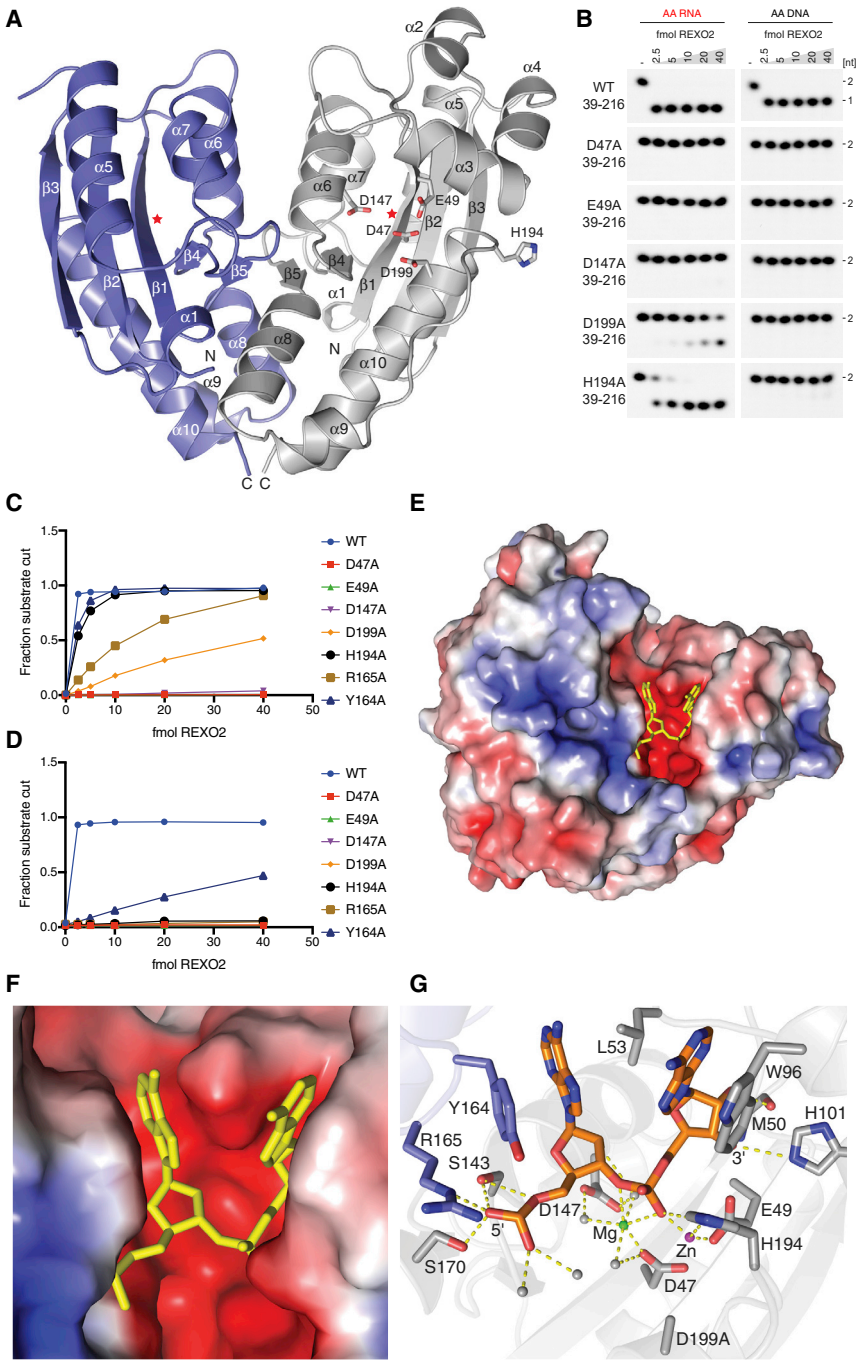

Figure 2. Structural Basis of REXO2 Substrate Specificity

(A) Front view of the overall structure of REXO2. Monomer A (gray) and monomer B (blue) are shown in cartoon representation with the DEDDh residues of monomer A shown as sticks. Stars indicate the active sites of monomer A and monomer B. Monomer B lacked clear density for regions encompassing helices α2–4 (residues 84–113) and a short loop corresponding to residues 189–192 and were therefore not built in the model.

(B) Activity of truncated REXO2 variants (amino acids 39–216) upon RNA or DNA AA dinucleotide substrates. Monophosphorylated radiolabeled substrate (10 fmol) was incubated with the indicated amounts of REXO2 at 37°C for 30 min, separated by 18% urea-PAGE, and imaged by autoradiography.

(C) Quantification of RNA degradation by REXO2 variants from (B).

(D) Quantification of DNA degradation by REXO2 variants as in (B).

(E) Surface representation of REXO2 with the RNA pApA dinucleotide (yellow) shown as sticks. The molecular surface is colored by the local electrostatic potential (blue, +5 kT; red, −5 kT).

(F) Enlargement of REXO2 active site with bound RNA pApA dinucleotide as in (E).

(G) The REXO2 active site. Residues interacting with the RNA pApA dinucleotide (orange) are shown as sticks and the polar bonds as yellow dashes. Zn^{2+} and Mg^{2+} are shown as pink and green spheres, respectively. Water molecules are shown as gray spheres.

from both the HSP and LSP was increased in the *Rexo2* knockout mice (Figures 6A and 6B), albeit only slightly, consistent with the finding that loss of REXO2 in the heart does not cause significant pathology. It is likely that highly proliferative tissues and cells are more affected by the loss of REXO2, as the clearance of dinucleotides would be more important at increased proliferation rates. Interestingly, PARE data showed that the most enriched 5′ end in the LSP region is positioned at the transcription initiation site and would give rise to transcripts with 5′-AG dinucleotides despite these being depleted overall in the knockout mice (Figure 5B). These findings suggest that transcription primed with AG dinucleotides is more efficient at the promoter than elsewhere in the genome.

To test the capacity of nanoRNAs to prime promoter-dependent transcription initiation, we used a reconstituted human *in vitro* transcription system with templates containing either the human LSP or HSP sequence. nanoRNAs that anneal to the promoter at the TSS were found to potently stimulate transcription initiation from both the LSP and HSP (Figures 6C and 6D). Similar to the observation of nanoRNA-primed transcription in the absence of a promoter (Figure S5E), the promoter-dependent effect was only observed using oligonucleotides containing AA at the 3′ end (Figures 6C and 6D). However, in contrast to results obtained with promoter-less templates, nanoRNAs are capable of priming promoter-dependent transcription using both linear templates and supercoiled templates (Figures 6C and 6D, compare lanes 3–8 with lanes 9–14). Although supercoiling was dispensable, nanoRNA-primed transcription remained absolutely dependent on the presence of

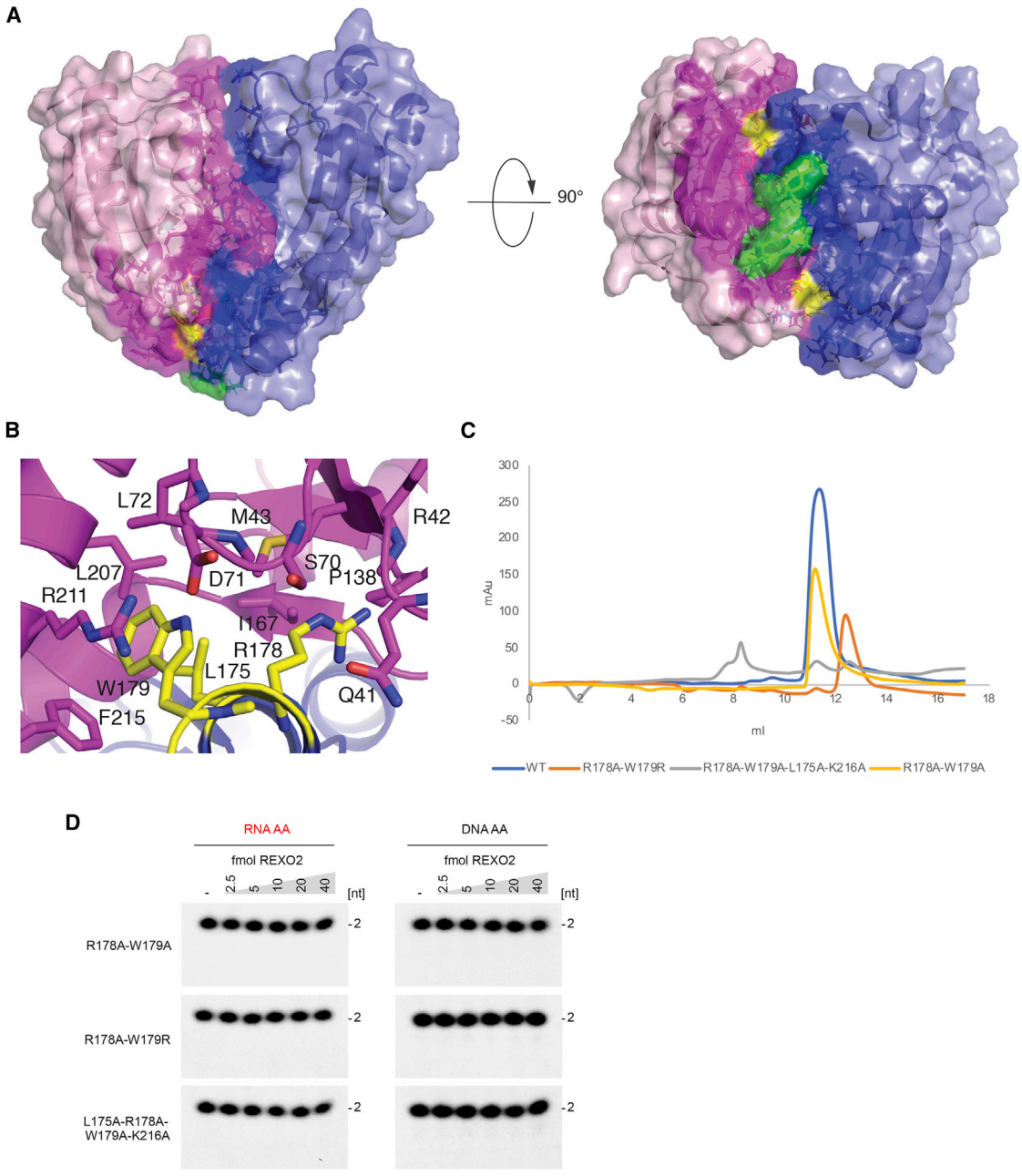

Figure 3. REXO2 Is an Obligate Homodimer

(A) Top and front views of the surface of REXO2 with monomer A (blue) and monomer B (pink), where the interface interacting residues are highlighted in darker colors. K216 is highlighted in green, and R178, W179, and L175 are highlighted in yellow.

(B) The R178-W179 binding pocket is shown in cartoon representation with R178, W179, and their interacting residues shown as sticks with the same color code as in (A).

(C) Gel filtration profiles of the REXO2 dimer mutants.

(D) Activity of REXO2 dimerization mutants upon RNA or DNA AA dinucleotides. Monophosphorylated radiolabeled substrate (10 fmol) was incubated with the indicated amounts of REXO2 protein at 37°C for 30 min, separated by 18% urea-PAGE, and imaged by autoradiography.

TFB2M (Figures S6A and S6B, compare lanes 3–8 with lanes 9–14), which contributes critically to promoter melting (Hillen et al., 2017; Morozov et al., 2015; Posse and Gustafsson, 2017; Sologub et al., 2009). The stimulation of transcription initiation by nanoRNAs was again observed at concentrations of nanoRNA much lower than that of ATP (Figures S6C and S6D) and was not seen using DNA primers (Figures S6E and S6F), indicating that nanoRNAs are used in preference to ATP to initiate transcription. Interestingly, the RNA 4-mer AAAA was able to prime transcription initiation from HSP despite not fully annealing to the promoter

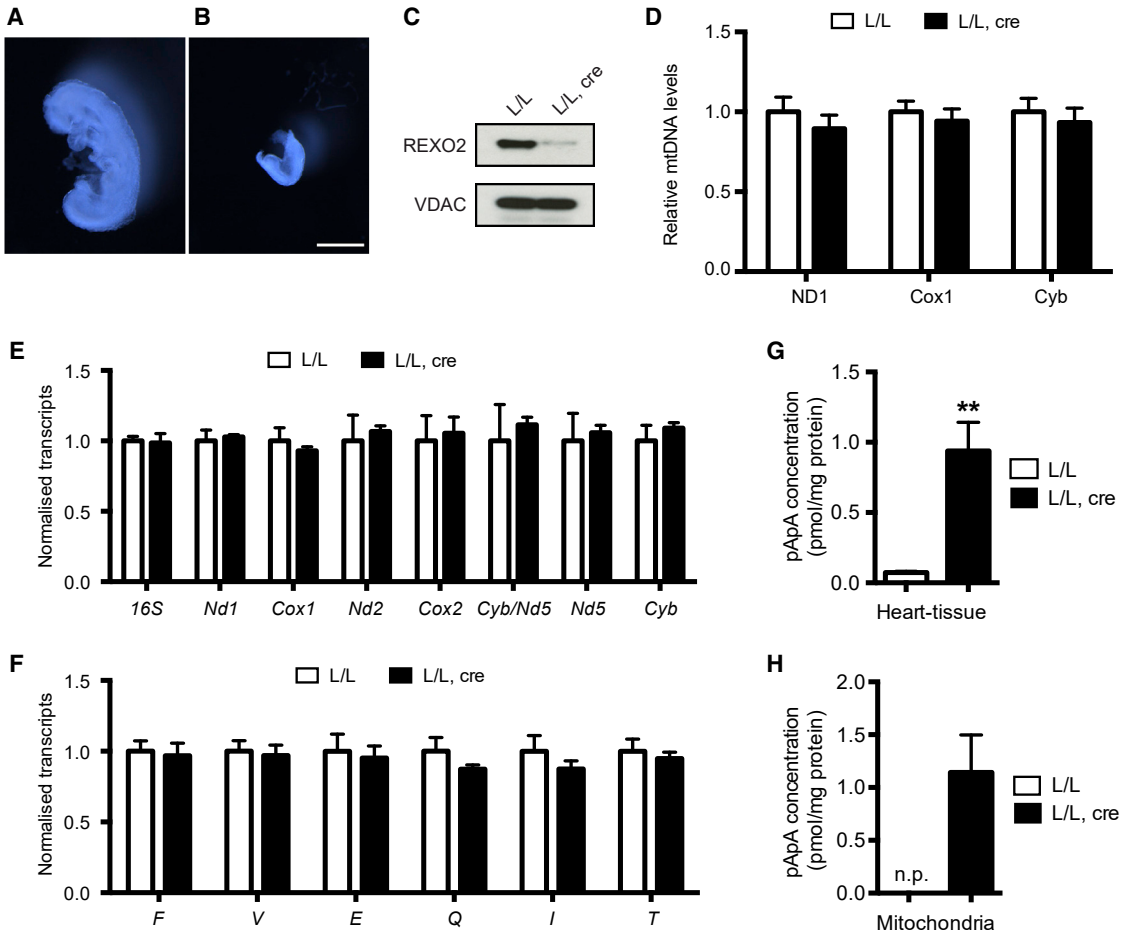

Figure 4. REXO2 Is Essential for Embryonic Development

(A and B) Morphology of *Rexo2*$^{+/+}$ (A) and *Rexo2*$^{-/-}$ (B) embryos at embryonic day 8.5. Scale bar, 500 μm.

(C) Western blot of REXO2 levels in hearts from control (L/L) and tissue-specific *Rexo2* knockout (L/L, cre) mice. VDAC is used as a loading control.

(D) mtDNA copy number in control and *Rexo2* knockout mice measured by qPCR using three TaqMan probe sets to different regions of the mitochondrial genome. mtDNA levels are normalized to the level of *Actin* and represent mean values from 3 independent experiments with total n = 15 mice for each group; error bars represent SEM.

(E) Mitochondrial mRNA steady-state levels in control and *Rexo2* knockout mice analyzed by northern blotting. Data are normalized to the level of *18S rRNA* and presented as mean values from 3 independent experiments with total n = 10 mice for each group; error bars represent SEM.

(F) mt-tRNA steady-state levels in control and *Rexo2* knockout mice analyzed by northern blotting. Data are normalized to the level of *5.8S rRNA* and presented as mean values from 3 independent experiments, with n = 15 mice for each group.

(G) Level of the pApA RNA dinucleotide in heart tissue from control and *Rexo2* knockout mice measured using LC-MS/MS. Data represent mean values from n = 3 mice for each group; error bars represent SEM, **$p < 0.01$.

(H) Level of the pApA RNA dinucleotide in isolated mitochondria from heart tissue of control and *Rexo2* knockout mice measured using LC-MS/MS. Data represent mean values from n = 3 mice for each group; error bars represent 1 SEM. n.p. indicates no peak.

sequence. Primer extension analysis of nanoRNA-primed transcription products was used to determine the exact site at which this nanoRNA anneals to the promoter during transcription initiation. This revealed a mixture of different RNA 5′ ends (Figure S7A), indicating that only the 3′ end of this nanoRNA is required to anneal in order to prime transcription, although transcript length may also be influenced by reiterative initiation at the TSS. We therefore also tested the ability of poly(A) nanoRNAs of different lengths to prime transcription from the LSP or HSP. All poly(A) sequences tested were capable of efficiently stimulating promoter-dependent transcription (Figures 6E, 6F, S7B, and S7C). The addition of the mitochondrial transcription elongation factor TEFM into nanoRNA-primed transcription reactions reduced the rate of pre-termination by the transcription complex, as expected (Jiang et al., 2019; Minczuk et al., 2011; Posse et al., 2015), but did not alter the rate of transcription initiation (Figures S7D and S7E, compare lanes 3–8 with lanes 9–14), indicating that TEFM does not contribute to transcription primed by nanoRNAs.

Loss of REXO2 Causes an mtRNA Processing Defect

We carried out RNA sequencing (RNA-seq) of RNA from *Rexo2* knockout mice and wild-type controls followed by

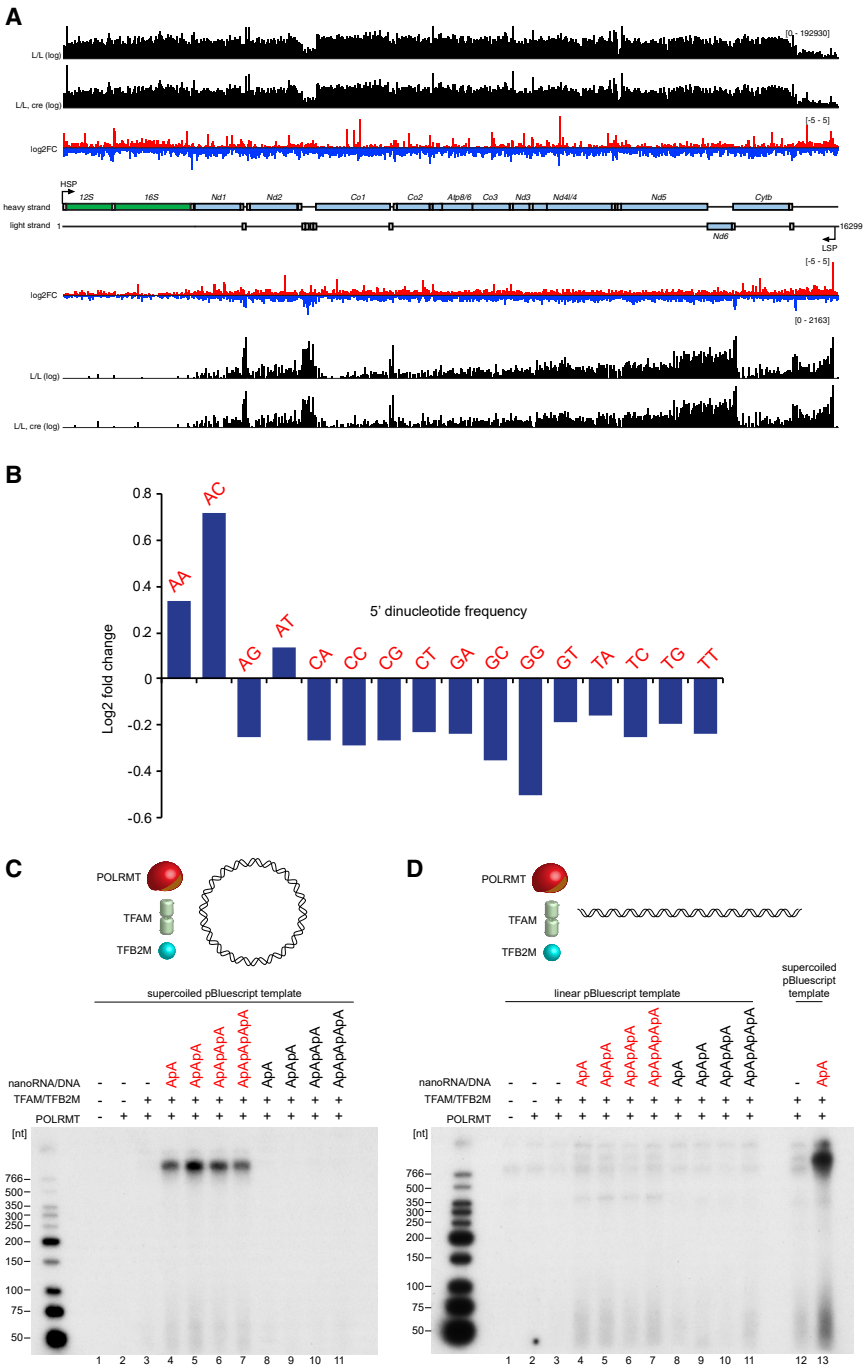

Figure 5. Loss of REXO2 Causes nanoRNA-Primed Non-canonical Mitochondrial Transcription Initiation

(A) A complete map of changes in 5′-end abundance (log2 fold change [knock out (KO)mean/control (Ctrl)mean]) from three control (L/L) and three *Rexo2* knockout (L/L, cre) mice on heavy (top) and light (bottom) strands. Mean increases are shown in red and mean decreases in blue. A schematic of the mitochondrial genome is displayed in the center; rRNAs are displayed in green, mRNAs in blue, tRNAs in gray, and the non-coding region (NCR) in black.

(B) Frequency of all possible dinucleotide combinations found at the 5′ ends of captured sequence tags in three control and *Rexo2* knockout mice.

(C) *In vitro* transcription reactions using supercoiled pBluescript II SK (+) DNA as a template. Reactions contain 20 μM ATP, CTP, and GTP; 1 μM UTP; 0.2 μCi ^{32}P α-UTP; and 20 μM of the indicated RNA or DNA oligonucleotide.

(D) *In vitro* transcription reactions as in (C) but containing BamHI-linearized pBluescript II SK (+) DNA as a template. Reactions using a supercoiled template (lanes 12 and 13) are included as a positive control.

differential expression analysis, which found no significant changes in the overall levels of mitochondrial transcripts and no large changes in nuclear gene expression (Table S2). We used the RNA-seq data to investigate if the increased presence of dinucleotides as a consequence of REXO2 loss can interfere with RNA processing and thereby cause an accumulation of mtRNA precursors. RNA-seq captures longer RNAs, such as mRNAs and rRNAs, but excludes mature tRNAs, providing a way to investigate the accumulation of tRNA-containing precursor transcripts in mitochondria since they are produced from the same polycistronic transcript (Rackham et al., 2016; Siira et al., 2018). We identified increases in the levels of precursor transcripts across the tRNA junctions that span each mRNA (Figure 7A) and rRNA (Figure 7B). To show that the accumulated transcripts were not only a consequence of increased transcription in the absence of REXO2, we also investigated the PARE datasets for changes in canonical cleavage sites across the entire mitochondrial transcriptome. In the REXO2 knockout mice, we identified decreases in the levels of 5′ tRNA canonical sites, whereas the levels of 3′ tRNA cleavage sites or non-canonical sites were either increased or not affected in the absence of REXO2 (Figure 7C). This suggests that an increased abundance of dinucleotides interferes with the processing of 5′ ends of mt-RNAs.

DISCUSSION

We have established REXO2 as a specialized dinucleotide-degrading enzyme in mammalian mitochondria. REXO2 acts as the final stage in mtRNA degradation, as the mononucleotides released by REXO2 can be recycled for further rounds of

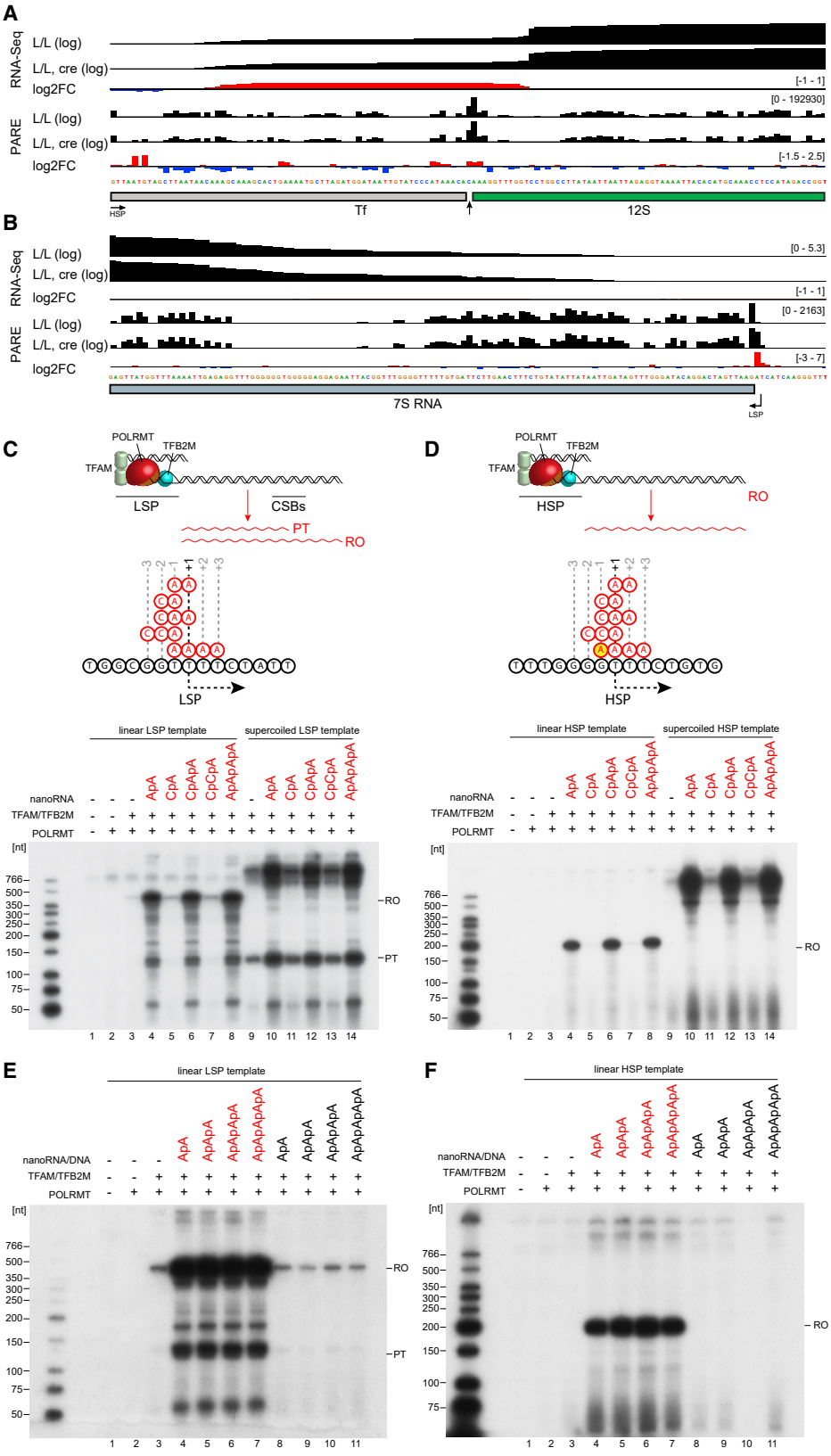

(legend on next page)

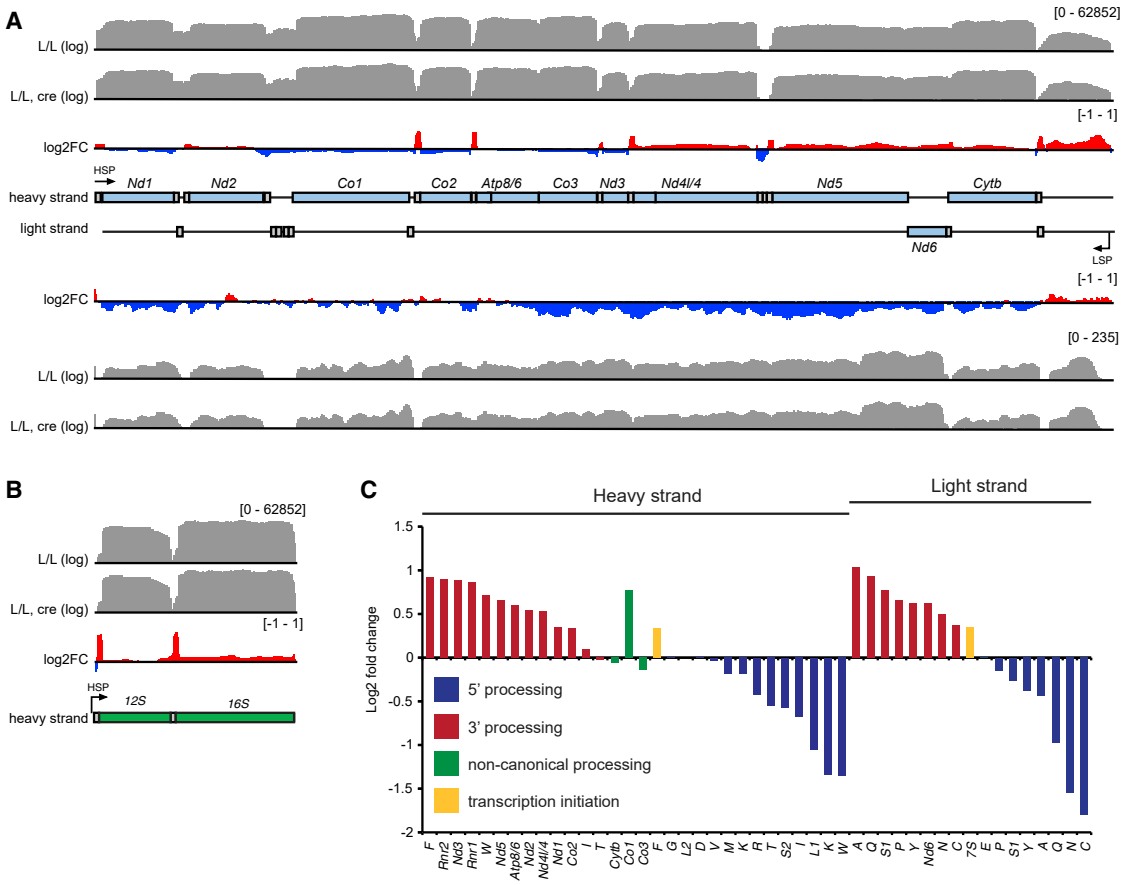

Figure 7. Loss of REXO2 Causes an RNA Processing Defect

(A and B) A complete map of mtRNA abundance and mean (log2 fold change [KOmean/Ctrlmean]) determined by RNA-seq coverage from control (n = 3) and *Rexo2* knockout (n = 3) mice on the heavy (upper) and light (lower) strand with the mtDNA genome positioned in the centre. Increases (red) and decreases (blue) are depicted for the coding regions (A) and rRNA regions (B).

(C) Changes in the levels of canonical mtRNA junctions were determined from the PARE datasets.

transcription. The best-characterized ribonuclease involved in mtRNA degradation, PNPase, is unable to degrade substrates of less than 4 nt in length (Lin et al., 2012) and therefore acts upstream of REXO2 in mtRNA degradation. However, it remains unclear whether these products of PNPase are further processed by other RNases or whether other enzymes also generate substrates for REXO2. The mitochondrial nuclease ExoG releases dinucleotides as reaction products and is active upon RNA (Szymanski et al., 2017; Wu et al., 2019) and so could potentially fulfill this role. Interestingly, a very recent study of *E. coli* Orn has similarly revealed a stark preference for diribonucleotide substrates (Kim et al., 2019), suggesting that oligoribonucleases have a more specialized and evolutionarily conserved role than previously understood. A second potential source of

Figure 6. Loss of REXO2 Causes Transcription Dysregulation at Mitochondrial Promoters

(A and B) Genome browser view (log scaled) of the abundance from three control (L/L) and three *Rexo2* knockout (L/L, cre) mice (mean normalized count) and relative changes (log2 fold change[KOmean/WTmean]) in RNA-seq and PARE libraries showing the abundance of 5′ ends mapped to the HSP (A) and LSP (B). The direction of transcription from the LSP and HSP is indicated, and the cleavage site between tRNA-Phe (TF) and 12S rRNA is indicated by an upward arrow.

(C) Schematic (top) shows the experimental setup of *in vitro* transcription reactions and complementarity between RNA oligonucleotides and the human LSP promoter sequence. Reactions (bottom) contain linearized or supercoiled LSP-containing plasmid template; 20 μM ATP, CTP, and GTP; 1 μM UTP; 0.2 μCi ^{32}P α-UTP; and 20 μM of the indicated RNA oligonucleotide (red). Oligonucleotide sequences are designed to anneal to the promoter sequence at the transcription start site as indicated. "RO" indicates the runoff transcription product, and "PT" indicates transcription products prematurely terminated at CSB2.

(D) *In vitro* transcription reactions as in (C) but containing linearized or supercoiled human HSP-containing plasmid as a template. A base in the AAAA RNA oligonucleotide (red) that is not complementary to the HSP sequence is shown in yellow in the schematic.

(E) *In vitro* transcription reactions as in (C) but using poly(A) RNA (red) or DNA (black) oligonucleotides.

(F) *In vitro* transcription reactions as in (D) but using poly(A) RNA (red) or DNA (black) oligonucleotides.

nanoRNAs in mitochondria are cycles of abortive transcription by POLRMT. Similarly to RNA polymerases in other systems, POLRMT engages in frequent rounds of abortive transcription initiation, releasing very short RNA products (Carpousis and Gralla, 1980; Gaspari et al., 2004; Luse and Jacob, 1987). As these RNAs are capable of annealing to the TSS, their rapid degradation is presumably required to prevent their use as primers.

The capacity of REXO2 to also efficiently degrade DNA dinucleotides (Figure 1C) suggests that REXO2 may also be involved in the terminal stage of mtDNA breakdown. Two recent studies have implicated the 3′–5′ exonuclease (proofreading) activity of the mitochondrial DNA polymerase POLγ and the exonuclease MGME1 in mtDNA degradation (Nissanka et al., 2018; Peeva et al., 2018). POLγ releases mononucleotides as reaction products (Kunkel and Soni, 1988), but MGME1 cleaves single-stranded DNA in a distributive manner to release short oligonucleotides (Kornblum et al., 2013; Szczesny et al., 2013), which may represent good substrates for REXO2; thus, the role of REXO2 in mtDNA metabolism warrants further investigation.

The RNA substrates of REXO2 were found to be potent stimulators of mitochondrial transcription, both from canonical promoters and non-canonical sites. In bacteria, it has been suggested that the priming of transcription by nanoRNAs is a physiological mechanism to regulate the activity of certain promoters, as the rate of nanoRNA-primed transcription varies according to the growth stage of the cells (Druzhinin et al., 2015; Vvedenskaya et al., 2012). The observation that nanoRNAs alter the rate of transcription initiation from both mitochondrial promoters (Figure 6) suggests that such a system is formally possible in mammalian mitochondria. However, the fact that the same nanoRNAs also prime transcription at non-canonical sites (Figure 5) makes such a system appear unlikely unless additional mechanisms exist to maintain promoter specificity *in vivo*. The stimulation of *in vitro* transcription initiation by nanoRNAs (Figure 6) suggests that the formation of the first phosphodiester bond by POLRMT represents a rate-limiting step for transcription initiation. This observation is in agreement with previous studies showing that the yeast mtRNA polymerase requires high ATP concentrations for the formation of the first phosphodiester bond, but not for elongation (Amiott and Jaehning, 2006a, 2006b). This ATP sensing mechanism could potentially couple transcription levels to respiration. For this model to function, AA dinucleotides, in which the first phosphodiester bond has already been formed, must be eliminated so that they do not serve as primers for transcription. REXO2 may serve this purpose.

The use of ATP as an initiating nucleotide leads to primary transcripts carrying a triphosphate at the 5′ end. In *E. coli*, this triphosphate acts to stabilize transcripts, while decapping of the RNA leads to the degradation of the resulting monophosphorylated transcript by RNase E (Deana et al., 2008). The possibility of a similar mechanism operating in mammalian mitochondria is precluded by the fact that the processing of polycistronic mtRNA precursors leads to the mature transcripts bearing a 5′ monophosphate (Ojala et al., 1981) and means that other mechanisms must be required to mark mitochondrial transcripts for degradation. Selective degradation of antisense mtRNAs has recently been suggested to be mediated by GRSF1 in conjunction with the degradosome (Pietras et al., 2018), but there is currently no known mechanism to distinguish between full-length and truncated sense-strand transcripts. This would presumably make it difficult to distinguish between mature transcripts and those initiated from non-canonical sites in mitochondria and helps to explain why transient depletion of REXO2 causes severe effects upon mitochondrial gene expression (Bruni et al., 2013).

The importance of a dinucleotidase activity is highlighted by the fact that REXO2 is essential for embryonic development (Figure 4). The finding that a heart-specific knockout of REXO2 was viable was therefore surprising but presumably reflects a greater requirement for this activity in proliferative tissues during development. The knockout of REXO2 results in embryonic lethality at around E8.5, similar to other genes involved in mtDNA maintenance and expression (Cerritelli et al., 2003; Larsson et al., 1998; Milenkovic et al., 2013). The role of the cytosolic form of REXO2 therefore appears less critical but would represent an interesting topic for future study.

STAR★METHODS

Detailed methods are provided in the online version of this paper and include the following:

- KEY RESOURCES TABLE
- LEAD CONTACT AND MATERIALS AVAILABILITY
- EXPERIMENTAL MODEL AND SUBJECT DETAILS
  - Mice
- METHOD DETAILS
  - Cloning and Purification of REXO2
  - Nuclease Assays
  - Crystallization and Structure Determination
  - Generation of Rexo2 Conditional Knockout Mice
  - Crude Mitochondrial Isolation
  - Western Blot Analysis
  - RNA Extraction, Quantitative PCR and Northern Blot Analysis
  - DNA Isolation, Quantification of mtDNA
  - Measurement of Dinucleotide Concentrations
  - Measurement of Nucleotide Concentrations
  - RNA Sequencing and Analyses
  - PARE and Analysis
  - Purification of Proteins for *in vitro* Transcription
  - *In vitro* Transcription Reactions
  - Primer Extension
- QUANTIFICATION AND STATISTICAL ANALYSIS
- DATA AND CODE AVAILABILITY

SUPPLEMENTAL INFORMATION

Supplemental Information can be found online at https://doi.org/10.1016/j.molcel.2019.09.010.

ACKNOWLEDGMENTS

The pETM-11 plasmid was a kind gift from the EMBL Protein Expression and Purification Facility. The crystallographic experiments were performed on

beamlines 14-1 (Bessy, Berlin, Germany) and ID29 (ESRF, Grenoble, France). We thank the Protein Science Facility at Karolinska Institutet, Stockholm, Sweden for support and providing instrumentation for protein crystallization. We would like to thank Professors R. Lightowlers and Z. Chrzanowska-Lightowlers for stimulating discussions throughout the project. The work described here was supported by the Swedish Research Council (2015-00418 to N.-G.L., 2018-02439 to M.F., 2018-02579 to A.C., and 2017-01257 to C.M.G.), the Swedish Cancer Foundation (2016-816 to M.F., 2016-599 to A.C., 2017-631 to C.M.G., and 2018-602 to N.-G.L.), the Knut and Alice Wallenberg Foundation (KAW 2017.0080 to M.F. and KAW 2016.0050 to N.G.L.), the European Research Council (683191 to M.F. and 741366 to N.-G.L.), and grants from the Swedish state under the agreement between the Swedish government and the county councils, the ALF agreement (ALFGBG-727491 to M.F., ALFGBG-728151 to C.M.G., and SLL2018.0471 to N.-G.L.), and grants and fellowships from the National Health and Medical Research Council, the Australian Research Council, and the Cancer Council of WA (to A.F. and O.R.). T.J.N. is the recipient of a Sir Henry Dale Fellowship jointly funded by the Wellcome Trust and the Royal Society (213464/Z/18/Z) and a Rosetrees and Stoneygate Trust Research Fellowship (M811).

AUTHOR CONTRIBUTIONS

T.J.N. performed *in vitro* nuclease and transcription assays. H.S. performed structure determination and analysis. S.J., C.K., and M.J. created and characterized mouse models. S.J.S., O.R., and A.F. performed sequencing and analysis. S.J. and V.K. measured dinucleotide levels, and S.S. and A.C. measured and analyzed NTP levels. H.S., J.H.K.K., and M.F. purified proteins. T.J.N., H.S., S.J., and A.F. wrote the manuscript (original draft). C.M.G. and N.-G.L. supervised the project. All authors contributed to editing the final manuscript.

DECLARATION OF INTERESTS

The authors declare no competing interests.

Received: April 30, 2019
Revised: July 12, 2019
Accepted: September 4, 2019
Published: October 3, 2019

REFERENCES

Adams, P.D., Afonine, P.V., Bunkóczi, G., Chen, V.B., Davis, I.W., Echols, N., Headd, J.J., Hung, L.W., Kapral, G.J., Grosse-Kunstleve, R.W., et al. (2010). PHENIX: a comprehensive Python-based system for macromolecular structure solution. Acta Crystallogr. D Biol. Crystallogr. *66*, 213–221.

Amiott, E.A., and Jaehning, J.A. (2006a). Mitochondrial transcription is regulated via an ATP "sensing" mechanism that couples RNA abundance to respiration. Mol. Cell *22*, 329–338.

Amiott, E.A., and Jaehning, J.A. (2006b). Sensitivity of the yeast mitochondrial RNA polymerase to +1 and +2 initiating nucleotides. J. Biol. Chem. *281*, 34982–34988.

Borowski, L.S., Dziembowski, A., Hejnowicz, M.S., Stepien, P.P., and Szczesny, R.J. (2013). Human mitochondrial RNA decay mediated by PNPase-hSuv3 complex takes place in distinct foci. Nucleic Acids Res. *41*, 1223–1240.

Bruni, F., Gramegna, P., Oliveira, J.M., Lightowlers, R.N., and Chrzanowska-Lightowlers, Z.M. (2013). REXO2 is an oligoribonuclease active in human mitochondria. PLoS ONE *8*, e64670.

Brzezniak, L.K., Bijata, M., Szczesny, R.J., and Stepien, P.P. (2011). Involvement of human ELAC2 gene product in 3′ end processing of mitochondrial tRNAs. RNA Biol. *8*, 616–626.

Burhenne, H., and Kaever, V. (2013). Quantification of cyclic dinucleotides by reversed-phase LC-MS/MS. Methods Mol. Biol. *1016*, 27–37.

Carpousis, A.J., and Gralla, J.D. (1980). Cycling of ribonucleic acid polymerase to produce oligonucleotides during initiation in vitro at the lac UV5 promoter. Biochemistry *19*, 3245–3253.

Cerritelli, S.M., Frolova, E.G., Feng, C., Grinberg, A., Love, P.E., and Crouch, R.J. (2003). Failure to produce mitochondrial DNA results in embryonic lethality in Rnaseh1 null mice. Mol. Cell *11*, 807–815.

Chu, L.Y., Agrawal, S., Chen, Y.P., Yang, W.S., and Yuan, H.S. (2019). Structural insights into nanoRNA degradation by human Rexo2. RNA *25*, 737–746.

Datta, A.K., and Niyogi, K. (1975). A novel oligoribonuclease of Escherichia coli. II. Mechanism of action. J. Biol. Chem. *250*, 7313–7319.

Deana, A., Celesnik, H., and Belasco, J.G. (2008). The bacterial enzyme RppH triggers messenger RNA degradation by 5′ pyrophosphate removal. Nature *451*, 355–358.

Dhir, A., Dhir, S., Borowski, L.S., Jimenez, L., Teitell, M., Rötig, A., Crow, Y.J., Rice, G.I., Duffy, D., Tamby, C., et al. (2018). Mitochondrial double-stranded RNA triggers antiviral signalling in humans. Nature *560*, 238–242.

Druzhinin, S.Y., Tran, N.T., Skalenko, K.S., Goldman, S.R., Knoblauch, J.G., Dove, S.L., and Nickels, B.E. (2015). A conserved pattern of primer-dependent transcription initiation in Escherichia coli and Vibrio cholerae revealed by 5′ RNA-seq. PLoS Genet. *11*, e1005348.

Emsley, P., and Cowtan, K. (2004). Coot: model-building tools for molecular graphics. Acta. Crystallogr. D. Biol. Crystallogr. *60*, 2126–2132.

Falkenberg, M., Gaspari, M., Rantanen, A., Trifunovic, A., Larsson, N.G., and Gustafsson, C.M. (2002). Mitochondrial transcription factors B1 and B2 activate transcription of human mtDNA. Nat. Genet. *31*, 289–294.

Gaspari, M., Falkenberg, M., Larsson, N.G., and Gustafsson, C.M. (2004). The mitochondrial RNA polymerase contributes critically to promoter specificity in mammalian cells. EMBO J. *23*, 4606–4614.

Ghosh, S., and Deutscher, M.P. (1999). Oligoribonuclease is an essential component of the mRNA decay pathway. Proc. Natl. Acad. Sci. USA *96*, 4372–4377.

Goldman, S.R., Sharp, J.S., Vvedenskaya, I.O., Livny, J., Dove, S.L., and Nickels, B.E. (2011). NanoRNAs prime transcription initiation in vivo. Mol. Cell *42*, 817–825.

Gustafsson, C.M., Falkenberg, M., and Larsson, N.G. (2016). Maintenance and expression of mammalian mitochondrial DNA. Annu. Rev. Biochem. *85*, 133–160.

Hillen, H.S., Morozov, Y.I., Sarfallah, A., Temiakov, D., and Cramer, P. (2017). Structural basis of mitochondrial transcription initiation. Cell *171*, 1072–1081.e1010.

Holzmann, J., Frank, P., Löffler, E., Bennett, K.L., Gerner, C., and Rossmanith, W. (2008). RNase P without RNA: identification and functional reconstitution of the human mitochondrial tRNA processing enzyme. Cell *135*, 462–474.

Jiang, S., Koolmeister, C., Misic, J., Siira, S., Kühl, I., Silva Ramos, E., Miranda, M., Jiang, M., Posse, V., Lytovchenko, O., et al. (2019). TEFM regulates both transcription elongation and RNA processing in mitochondria. EMBO Rep. *20*, 48101.

Kabsch, W. (1993). Automatic processing of rotation diffraction data from crystals of initially unknown symmetry and cell constants. J. Appl. Cryst. *26*, 795–800.

Kim, S.K., Lormand, J.D., Weiss, C.A., Eger, K.A., Turdiev, H., Turdiev, A., Winkler, W.C., Sondermann, H., and Lee, V.T. (2019). A dedicated diribonucleotidase resolves a key bottleneck for the terminal step of RNA degradation. eLife *8*, e46313.

Kornblum, C., Nicholls, T.J., Haack, T.B., Schöler, S., Peeva, V., Danhauser, K., Hallmann, K., Zsurka, G., Rorbach, J., Iuso, A., et al. (2013). Loss-of-function mutations in MGME1 impair mtDNA replication and cause multisystemic mitochondrial disease. Nat. Genet. *45*, 214–219.

Kunkel, T.A., and Soni, A. (1988). Exonucleolytic proofreading enhances the fidelity of DNA synthesis by chick embryo DNA polymerase-gamma. J. Biol. Chem. *263*, 4450–4459.

Langmead, B., and Salzberg, S.L. (2012). Fast gapped-read alignment with Bowtie 2. Nat. Methods *9*, 357–359.

Larsson, N.G., Wang, J., Wilhelmsson, H., Oldfors, A., Rustin, P., Lewandoski, M., Barsh, G.S., and Clayton, D.A. (1998). Mitochondrial transcription factor A is necessary for mtDNA maintenance and embryogenesis in mice. Nat. Genet. *18*, 231–236.

Liao, Y., Smyth, G.K., and Shi, W. (2014). featureCounts: an efficient general purpose program for assigning sequence reads to genomic features. Bioinformatics *30*, 923–930.

Lin, C.L., Wang, Y.T., Yang, W.Z., Hsiao, Y.Y., and Yuan, H.S. (2012). Crystal structure of human polynucleotide phosphorylase: insights into its domain function in RNA binding and degradation. Nucleic Acids Res. *40*, 4146–4157.

Love, M.I., Huber, W., and Anders, S. (2014). Moderated estimation of fold change and dispersion for RNA-seq data with DESeq2. Genome Biol. *15*, 550.

Lovell, S.C., Davis, I.W., Arendall, W.B., 3rd, de Bakker, P.I., Word, J.M., Prisant, M.G., Richardson, J.S., and Richardson, D.C. (2003). Structure validation by Calpha geometry: phi,psi and Cbeta deviation. Proteins *50*, 437–450.

Luse, D.S., and Jacob, G.A. (1987). Abortive initiation by RNA polymerase II in vitro at the adenovirus 2 major late promoter. J. Biol. Chem. *262*, 14990–14997.

McCoy, A.J., Grosse-Kunstleve, R.W., Storoni, L.C., and Read, R.J. (2005). Likelihood-enhanced fast translation functions. Acta Crystallogr. D Biol. Crystallogr. *61*, 458–464.

Mechold, U., Ogryzko, V., Ngo, S., and Danchin, A. (2006). Oligoribonuclease is a common downstream target of lithium-induced pAp accumulation in Escherichia coli and human cells. Nucleic Acids Res. *34*, 2364–2373.

Mechold, U., Fang, G., Ngo, S., Ogryzko, V., and Danchin, A. (2007). YtqI from Bacillus subtilis has both oligoribonuclease and pAp-phosphatase activity. Nucleic Acids Res. *35*, 4552–4561.

Mercer, T.R., Neph, S., Dinger, M.E., Crawford, J., Smith, M.A., Shearwood, A.M., Haugen, E., Bracken, C.P., Rackham, O., Stamatoyannopoulos, J.A., et al. (2011). The human mitochondrial transcriptome. Cell *146*, 645–658.

Milenkovic, D., Matic, S., Kühl, I., Ruzzenente, B., Freyer, C., Jemt, E., Park, C.B., Falkenberg, M., and Larsson, N.G. (2013). TWINKLE is an essential mitochondrial helicase required for synthesis of nascent D-loop strands and complete mtDNA replication. Hum. Mol. Genet. *22*, 1983–1993.

Minczuk, M., He, J., Duch, A.M., Ettema, T.J., Chlebowski, A., Dzionek, K., Nijtmans, L.G., Huynen, M.A., and Holt, I.J. (2011). TEFM (c17orf42) is necessary for transcription of human mtDNA. Nucleic Acids Res. *39*, 4284–4299.

Morozov, Y.I., Agaronyan, K., Cheung, A.C., Anikin, M., Cramer, P., and Temiakov, D. (2014). A novel intermediate in transcription initiation by human mitochondrial RNA polymerase. Nucleic Acids Res. *42*, 3884–3893.

Morozov, Y.I., Parshin, A.V., Agaronyan, K., Cheung, A.C., Anikin, M., Cramer, P., and Temiakov, D. (2015). A model for transcription initiation in human mitochondria. Nucleic Acids Res. *43*, 3726–3735.

Nguyen, L.H., Erzberger, J.P., Root, J., and Wilson, D.M., 3rd (2000). The human homolog of Escherichia coli Orn degrades small single-stranded RNA and DNA oligomers. J. Biol. Chem. *275*, 25900–25906.

Nissanka, N., Bacman, S.R., Plastini, M.J., and Moraes, C.T. (2018). The mitochondrial DNA polymerase gamma degrades linear DNA fragments precluding the formation of deletions. Nat. Commun. *9*, 2491.

Niyogi, S.K., and Datta, A.K. (1975). A novel oligoribonuclease of Escherichia coli. I. Isolation and properties. J. Biol. Chem. *250*, 7307–7312.

Ojala, D., Montoya, J., and Attardi, G. (1981). tRNA punctuation model of RNA processing in human mitochondria. Nature *290*, 470–474.

Peeva, V., Blei, D., Trombly, G., Corsi, S., Szukszto, M.J., Rebelo-Guiomar, P., Gammage, P.A., Kudin, A.P., Becker, C., Altmüller, J., et al. (2018). Linear mitochondrial DNA is rapidly degraded by components of the replication machinery. Nat. Commun. *9*, 1727.

Pietras, Z., Wojcik, M.A., Borowski, L.S., Szewczyk, M., Kulinski, T.M., Cysewski, D., Stepien, P.P., Dziembowski, A., and Szczesny, R.J. (2018). Dedicated surveillance mechanism controls G-quadruplex forming non-coding RNAs in human mitochondria. Nat. Commun. *9*, 2558.

Posse, V., and Gustafsson, C.M. (2017). Human mitochondrial transcription factor B2 is required for promoter melting during initiation of transcription. J. Biol. Chem. *292*, 2637–2645.

Posse, V., Shahzad, S., Falkenberg, M., Hällberg, B.M., and Gustafsson, C.M. (2015). TEFM is a potent stimulator of mitochondrial transcription elongation in vitro. Nucleic Acids Res. *43*, 2615–2624.

Quinlan, A.R., and Hall, I.M. (2010). BEDTools: a flexible suite of utilities for comparing genomic features. Bioinformatics *26*, 841–842.

R Development Core Team (2010). R: A Language and Environment for Statistical Computing (R Foundation for Statistical Computing). http://www.R-project.org.

Rackham, O., and Filipovska, A. (2014). Analysis of the human mitochondrial transcriptome using directional deep sequencing and parallel analysis of RNA ends. Methods Mol. Biol. *1125*, 263–275.

Rackham, O., Busch, J.D., Matic, S., Siira, S.J., Kuznetsova, I., Atanassov, I., Ermer, J.A., Shearwood, A.M., Richman, T.R., Stewart, J.B., et al. (2016). Hierarchical RNA processing is required for mitochondrial ribosome assembly. Cell Rep. *16*, 1874–1890.

Sanchez, M.I., Mercer, T.R., Davies, S.M., Shearwood, A.M., Nygård, K.K., Richman, T.R., Mattick, J.S., Rackham, O., and Filipovska, A. (2011). RNA processing in human mitochondria. Cell Cycle *10*, 2904–2916.

Shi, Y., Dierckx, A., Wanrooij, P.H., Wanrooij, S., Larsson, N.G., Wilhelmsson, L.M., Falkenberg, M., and Gustafsson, C.M. (2012). Mammalian transcription factor A is a core component of the mitochondrial transcription machinery. Proc. Natl. Acad. Sci. USA *109*, 16510–16515.

Siira, S.J., Rossetti, G., Richman, T.R., Perks, K., Ermer, J.A., Kuznetsova, I., Hughes, L., Shearwood, A.J., Viola, H.M., Hool, L.C., et al. (2018). Concerted regulation of mitochondrial and nuclear non-coding RNAs by a dual-targeted RNase Z. EMBO Rep. *19*, e46198.

Smart, O.S., Womack, T.O., Flensburg, C., Keller, P., Paciorek, W., Sharff, A., Vonrhein, C., and Bricogne, G. (2012). Exploiting structure similarity in refinement: automated NCS and target-structure restraints in BUSTER. Acta Crystallogr. D Biol. Crystallogr. *68*, 368–380.

Sologub, M., Litonin, D., Anikin, M., Mustaev, A., and Temiakov, D. (2009). TFB2 is a transient component of the catalytic site of the human mitochondrial RNA polymerase. Cell *139*, 934–944.

Szczesny, R.J., Borowski, L.S., Brzezniak, L.K., Dmochowska, A., Gewartowski, K., Bartnik, E., and Stepien, P.P. (2010). Human mitochondrial RNA turnover caught in flagranti: involvement of hSuv3p helicase in RNA surveillance. Nucleic Acids Res. *38*, 279–298.

Szczesny, R.J., Hejnowicz, M.S., Steczkiewicz, K., Muszewska, A., Borowski, L.S., Ginalski, K., and Dziembowski, A. (2013). Identification of a novel human mitochondrial endo-/exonuclease Ddk1/c20orf72 necessary for maintenance of proper 7S DNA levels. Nucleic Acids Res. *41*, 3144–3161.

Szymanski, M.R., Yu, W., Gmyrek, A.M., White, M.A., Molineux, I.J., Lee, J.C., and Yin, Y.W. (2017). A domain in human EXOG converts apoptotic endonuclease to DNA-repair exonuclease. Nat. Commun. *8*, 14959.

Vvedenskaya, I.O., Sharp, J.S., Goldman, S.R., Kanabar, P.N., Livny, J., Dove, S.L., and Nickels, B.E. (2012). Growth phase-dependent control of transcription start site selection and gene expression by nanoRNAs. Genes Dev. *26*, 1498–1507.

Watt, D.L., Buckland, R.J., Lujan, S.A., Kunkel, T.A., and Chabes, A. (2016). Genome-wide analysis of the specificity and mechanisms of replication infidelity driven by imbalanced dNTP pools. Nucleic Acids Res. *44*, 1669–1680.

Wu, C.C., Lin, J.L.J., Yang-Yen, H.F., and Yuan, H.S. (2019). A unique exonuclease ExoG cleaves between RNA and DNA in mitochondrial DNA replication. Nucleic Acids Res. *47*, 5405–5419.

STAR★METHODS

KEY RESOURCES TABLE

REAGENT or RESOURCE	SOURCE	IDENTIFIER
Antibodies		
Rabbit polyclonal anti-REXO2	Abcam	Cat# ab206694
Anti-VDAC	Abcam	Cat# ab14734; RRID:AB_443084
Bacterial and Virus Strains		
Rosetta 2 Competent Cells	Merck Millipore	Cat#71402
Single Step (KRX) Competent Cells	Promega	Cat#L3002
Autographa californica nuclear polyhedrosis virus	Clontech	Cat#631401
Chemicals, Peptides, and Recombinant Proteins		
Human REXO2-6His WT	This paper	N/A
Human REXO2 39-216, WT and point mutants	This paper	N/A
Human POLRMT	Falkenberg et al. (2002)	N/A
Human TFAM	Falkenberg et al. (2002)	N/A
Human TFB2M	Falkenberg et al. (2002)	N/A
Human TEFM	Posse et al. (2015)	N/A
Critical Commercial Assays		
HIS-Select Nickel Affinity Gel	Sigma-Aldrich	Cat#P6611
HiLoad 16/600 Superdex 200 pg Gel Filtration Columns	GE Healthcare	Cat#28989335
HiTrap Q HP	GE Healthcare	Cat#29051325
Superdex 75 Increase Size Exclusion Columns	GE Healthcare	Cat#29148721
Amersham ECL Western Blotting Detection Reagent	GE Healthcare	Cat# RPN2106
High molecular weight native maker kit	GE Healthcare	Cat# 17-0445-01
Trizol reagent	Thermo Fisher	Cat# 15596026
High-Capacity cDNA Reverse Transcription Kit	Thermo Fisher	Cat#4368814
TaqMan Universal Mast er Mix II, with UNG	Thermo Fisher	Cat#4440038
T4 Polynucleotide Kinase	New England Biolabs	Cat# M0201
RNase A, DNase and protease-free	Thermo Fisher	Cat# EN0531
DNeasy Blood and Tissue Kit	QIAGEN	Cat# 69506
Ribo-Zero rRNA Removal Kit	Illumina	Cat#MRZH116
Superscript II Reverse Transcriptase Kit	Thermo Fisher	Cat#19064014
miRNeasy Mini Kit	QIAGEN	Cat# 217004
TURBO DNA-free Kit	Thermo Fisher	Cat# AM1907
Platinum SYBR Green qPCR supermix-UDG	Thermo Fisher	Cat# 11733046
Prime-It II Random Primer Labeling Kit	Agilent	Cat# 300385
Deposited Data		
REXO2 (apo) structure	This paper	PDB: 6RCI
REXO2 (pApA-bound) structure	This paper	PDB: 6RCL
REXO2 (dAdA-bound) structure	This paper	PDB: 6RCN
RNA-seq and PARE data	This paper	GEO: GSE129707
Original image data	This paper	https://doi.org/10.17632/ss68bdtccy.1

(*Continued on next page*)

Continued

REAGENT or RESOURCE	SOURCE	IDENTIFIER
Experimental Models: Cell Lines		
Spodoptera frugiperda: Sf9 Cells	Clontech	Cat#631402
Experimental Models: Organisms/Strains		
Mouse: C57BL/6N *Rexo2*$^{+/-}$	This paper	N/A
Mouse: C57BL/6N *Rexo2*$^{loxP/loxP}$, +/*Ckmm-cre*	This paper	N/A
Oligonucleotides		
2-5-mer RNA and DNA oligos, see Table S3	This paper	N/A
Primer for qPCR, see Table S3	This paper	N/A
Primers for Northern blot probes, see Table S3	This paper	N/A
pApA, standard for mass spectrometry	Biolog	Cat#P033
hLSP_PEx primer, see Table S3	This paper	N/A
Recombinant DNA		
Plasmid: pETM-11-REXO2	This paper	N/A
Plasmid: pBluescript II SK(+)	Stratagene	Cat#212205
Plasmid: pUC18 m.1-477	Falkenberg et al. (2002)	N/A
Plasmid: pUC18 m.499-742	Falkenberg et al. (2002)	N/A
Software and Algorithms		
XDS	MPI for Medical Research, Heidelberg	http://xds.mpimf-heidelberg.mpg.de/
Phaser	Cambridge Institute for Medical Research	https://www.phaser.cimr.cam.ac.ukindex.php/Phaser_Crystallographic_Software
Autobuild	PHENIX Online	https://www.phenix-online.org/documentation/reference/autobuild.html
COOT	MRC LMB	https://www2.mrc-lmb.cam.ac.uk/personal/pemsley/coot/
Buster	Global Phasing	https://www.globalphasing.com/buster/
MolProbity	Duke University	http://molprobity.biochem.duke.edu/
Pymol	Schrödinger	https://pymol.org/2/
Bowtie 2	Johns Hopkins University	http://bowtie-bio.sourceforge.net/bowtie2/index.shtml
Bedtools	University of Utah	https://bedtools.readthedocs.io/en/latest/
featureCounts	Walter and Eliza Hall Institute	http://bioinf.wehi.edu.au/featureCounts/
DESeq 2	Bioconductor	https://bioconductor.org/packages/release/bioc/html/DESeq2.html
CLC Genomics Workbench	QIAGEN	https://www.qiagenbioinformatics.com/products/clc-genomics-workbench/
R	The R Project for Statistical Computing	https://www.r-project.org/
MultiGauge V3.0	Fujifilm	N/A
GraphPad Prism	GraphPad Software	https://www.graphpad.com/scientific-software/prism/
ImageQuant TL 8.1	GE Healthcare	http://www.gelifesciences.com/en/us/shop/protein-analysis/molecular-imaging-for-proteins/imaging-software/imagequant-tl-8-1-p-00110

LEAD CONTACT AND MATERIALS AVAILABILITY

Requests for reagents and resources should be directed to, and will be fulfilled by, the lead contact, Claes Gustafsson (claes.gustafsson@medkem.gu.se).

EXPERIMENTAL MODEL AND SUBJECT DETAILS

Mice

All mice in this study had an inbred C57BL/6N background. Animal studies were approved by the animal welfare ethics committee and performed in compliance with National and European law.

METHOD DETAILS

Cloning and Purification of REXO2

Codon-optimized (Genscript) DNA constructs corresponding to amino acids 39-216 of human REXO2 was cloned in a pETM-11 vector (EMBL). REXO2 was expressed in Rosetta 2 cells (EMD chemicals) by autoinduction in Magic media (Invitrogen) at 25°C for 16 hours. After lysis, the proteins were purified over a His-Select Ni^{2+} (Sigma-Aldrich) resin and dialyzed against H-0.2 (25 mM Tris-HCl [pH 7.8], 0.5 mM EDTA, 10% glycerol, 1 mM DTT, 0.2 M NaCl) after the addition of TEV protease at a 1:10 protease:protein ratio. Further purification was conducted over a HiLoad 16/60 Superdex 200 pg gel filtration column (GE Healthcare) in buffer H-0.2 lacking glycerol and concentrated using Vivaspin concentrators (10,000 Da MWCO, Sartorius). Dimerization mutants were dialyzed against H-0.1 after the Ni^{2+} purification step and further purified over a Hitrap-Q (1 ml) column equilibrated in H-0.1. After washing with H-0.1 the proteins were eluted with a 30 mL linear gradient between H-0.1 and H-1.0. The dimerization state was determined on a Superdex 75 increase (GE Healthcare) column equilibrated in H-0.5 lacking glycerol.

Nuclease Assays

REXO2 nuclease assays were performed according to the method of Nguyen et al. (2000). RNA and DNA substrates were 5′ end labeled using T4 polynucleotide kinase (NEB) according to the manufacturer's instructions and purified using MicroSpin G-25 columns (GE Healthcare). Nuclease reactions (10 μl) contained 10 fmol of labeled substrate, 50 mM HEPES-KOH pH 7.4, 50 mM KCl, 10 mM MnCl2, 0.01% Triton X-100, 10% glycerol, 0.1 mM DTT and the indicated amount of REXO2 protein prepared in dilution buffer (200 mM NaCl, 100 μg/ml BSA, 0.5 mM EDTA, 20 mM Tris-Cl pH 8, 1 mM DTT, 10% glycerol). Reactions were incubated at 37°C for 30 min then stopped by the addition of 10 μl loading buffer (98% formamide, 10 mM EDTA, 0.025% xylene cyanol and 0.025% bromophenol blue) and separated by 18% denaturing PAGE. Gels were exposed to storage phosphor screens and scanned using a Fujifilm FLA-7000 for quantification, or exposed to X-ray film.

Crystallization and Structure Determination

Crystals of REXO2 were grown at 23°C by the hanging drop vapor diffusion method by mixing 1 μL protein (20 mg/ml) with an equal volume of reservoir solution (100 mM HEPES pH 7.0, 200 mM sodium malonate, and 20% polyethylene glycol 3350). For soaking experiments, REXO2 D199A mutant crystals were incubated in a fresh drop containing 100 mM MES pH 5.5, 200 mM sodium malonate, 20% polyethylene glycol 3350, 20 mM $MgCl_2$, 1 mM $ZnCl_2$, 12% glycerol and 1 mM oligonucleotide for 30-60 min. Diffraction data were collected at beamlines 14-1 (Bessy, Berlin, Germany) and ID29 (ESRF, Grenoble, France). The data (Table 1) were processed with XDS (Kabsch, 1993) and the structure was solved by molecular replacement with Phaser (McCoy et al., 2005), using ORN from *Escherichia coli* (PDB: 1YTA) as search model. The molecular replacement solution was used as a starting model for building by Autobuild (Adams et al., 2010) that was further improved by manual building in COOT (Emsley and Cowtan, 2004) interspersed with refinement in Buster (Smart et al., 2012), which rendered a final model (Table 1) that had no Ramachandran outliers as assessed by MolProbity (Lovell et al., 2003). A dataset collected near the peak of anomalous scattering by zinc (1.28 Å) was collected for the DNA bound REXO2. Both dinucleotide bound structures were solved by molecular replacement using the apo structure as the search model. Figures were prepared with Pymol (Schrödinger).

Generation of Rexo2 Conditional Knockout Mice

The *Rexo2* conditional knockout mice were generated by Taconic Artemis. Exons 3-5 of the *Rexo2* locus were flanked by *loxP* sites, and two positive selection markers including a neomycin resistance cassette (NeoR) flanked by *Frt* sites and a puromycin resistance cassette (PuroR) flanked by *F3* sites were introduced in intron 2 and intron 5, respectively. The NeoR and PuroR were removed by the mating of $Rexo2^{+/loxP\text{-}Neo\text{-}Puro}$ mice with transgenic mice ubiquitously expressing *Flp*-recombinase. After the *Flp* recombination, the resulting $Rexo2^{+/loxP}$ mice were subsequently crossed with transgenic mice ubiquitously expressing cre-recombinase under the control of (1) the *β -actin* promoter (+/*β -actin*) to generate *Rexo2* heterozygous knockout mice ($Rexo2^{+/-}$) or (2) the muscle creatinine kinase promoter (+/*Ckmm-cre*) to generate heart and skeletal muscle *Rexo2* conditional knockout mice ($Rexo2^{loxP/loxP}$, +/*Ckmm-cre*; L/L, cre).

Crude Mitochondrial Isolation

Mitochondria from mouse heart were isolated by differential centrifugation using isolation buffer (320 mM sucrose, 10 mM Tris-HCl, pH 7.4 and 1 mM EDTA), supplemented with protease inhibitor (Roche). Hearts were homogenized using a Potter-Elvehjem homogenizer on ice (15 strokes, 500 rpm). Nuclei and cell debris were pelleted at 1,000 g for 10 minutes at 4°C. The supernatant was centrifuged at 10,000 g for 10 min at 4°C. The differential centrifugation was repeated twice to obtain the crude mitochondria.

Western Blot Analysis

Crude mitochondria or total protein (10-30 μg) were resuspended in 1 x NuPAGE LDS Sample Buffer. Mitochondrial proteins were separated by SDS-PAGE (4%–12% Bis-Tris Protein Gels; Invitrogen) and transferred onto Polyvinylidene difluoride (PVDF) membranes (Merck Millipore). Immunoblotting was performed using standard procedures and developed using ECL Reagent.

RNA Extraction, Quantitative PCR and Northern Blot Analysis

RNA was extracted from heart using Trizol reagent (Thermo Fisher Scientific) according to the manufacturer's instructions, then treated with TURBO DNA-free DNase (Thermo Fisher Scientific). For qPCR expression analysis, cDNA was reversed transcribed from 1 μg total RNA using High-Capacity cDNA Reverse Transcription Kit (Thermo Fisher Scientific). Quantitative PCR was performed in a QuantStudio 6 Flex Real-Time PCR System (Life Technologies), using (1) TaqMan Universal Master Mix II, with UNG to quantify mitochondrial transcripts (mt-rRNAs and mt-mRNAs) and *Actin*, and (2) Platinum SYBR Green qPCR supermix-UDG (Invitrogen) to quantify the levels of *Rexo2* and *Actin*. Primer sequences are shown in Table S3.

For northern blotting, 5 μg of total RNA was separated in either 1% MOPS-formaldehyde agarose gels to detect mt-mRNAs and mt-rRNAs or neutral 10% polyacrylamide gels to detect mt-tRNAs. Separated RNAs were then transferred to Hybond-N+ membranes (GE Healthcare) and hybridized with (1) randomly [^{32}P] dCTP-labeled dsDNA probes, following the Prime-It II Random Primer Labeling Kit (Agilent), to detect mt-mRNAs (except *Nd6*), mt-rRNAs, *18S rRNA* and *5.8S rRNA*; (2) strand-specific oligonucleotide probes labeled with [^{32}P] dATP, using T4 Polynucleotide Kinase (New England Biolabs), to detect mt-tRNAs. Radioactive signals were captured in a phosphorImager screen and was quantified using a Typhoon 7000 FLA and the ImageQuant TL 8.1 software (GE Healthcare).

DNA Isolation, Quantification of mtDNA

Genomic DNA from mouse heart was isolated with the DNeasy Blood and Tissue Kit (QIAGEN) following manufacturer's instructions, followed by treatment with RNase A. Mitochondrial DNA copy number was measured by quantitative PCR using 5 ng of DNA in a QuantStudio 6 Flex Real-Time PCR System using TaqMan Universal Master Mix II. The TaqMan assays were used for the detection of mtDNA were *Nd1*, *Cox1* and *Cyb*. *18S* was used to normalize for nuclear input.

Measurement of Dinucleotide Concentrations

Quantification of the linear dinucleotide pApA was performed by HPLC-coupled tandem mass spectrometry (LC-MS/MS), based on our standard method (Burhenne and Kaever, 2013). Crude mitochondria were suspended in 1200 μl ice-cold extraction solution (acetonitrile/methanol/water, 2:2:1 v/v/v, HPLC grade), or 75 mg heart tissue was mixed with 600 μl ice-cold extraction solution. Heart tissue was homogenized using a FastPrep FP120 (Thermo Savant) at 4.5 m/s for 40 s. Extracted suspensions were transferred to a new tube, and the tube used for homogenization was washed with 2 × 300 μl extraction solution and combined with the homogenate. Samples were extracted by incubation at 95°C for 10 minutes, then stored at −20°C overnight to enforce protein precipitation. Precipitated protein was pelleted by centrifugation at 20,800 g for 10 minutes at 4°C, and the supernatant dried using a SpeedVac. The dried extracts were dissolved in 150 μl H_2O and HPLC separation was conducted by a Shimadzu LC-10 series chromatograph equipped with an EC 50/3 Nucleodur C18 Pyramid column (Macherey & Nagel), additionally coupled with a C18 security guard (Phenomenex) and a 0.5 μm column saver (Supelco). For separation of pApA, gradient elution at 30°C was used (solvent A, 10 mM ammonium acetate/0.1% acetic acid; solvent B, methanol; 0 to 4 min, 100% A; 4 to 7.3 min, 90% A; 7.3 to 8.3 min, 90% A; 8.3 to 11 min, 70% A; 11 to 11.1 min, 100% A, 11.1 to 13 min, 100%A). Retention time of pApA was 6.6 min. MS/MS analysis was carried out by an API4000 mass spectrometer (Sciex) operating in positive electrospray and multiple reaction monitoring mode. As main mass transitions [M+H]+ for pApA m/z 676.9 to 136.0 (quantifier) and 676.9 to 119.1 (identifier) were recorded. Quantification was done in comparison to authentic pApA (Biolog) and tenofovir as internal standard. For quantification of dinucleotide levels, precipitated cell pellets were dissolved in 800 μl of 0.1 N NaOH and heated to 95°C for 15 minutes. Protein concentrations were determined using a BCA assay.

Measurement of Nucleotide Concentrations

Nucleotides from freshly dissected heart tissues and from isolated mitochondria were extracted by homogenization in 250 μl of ice-cold 12% TCA-15 mM MgCl2 solution followed by two rounds of neutralization steps using Freon-Trioctylamine mix. For determining the NTP levels, 50 μl of heart tissue samples or 150 μl of mitochondrial samples were analyzed by HPLC as described in Watt et al. (2016). NTP levels were normalized to the total protein content in each sample, determined using a BCA assay.

RNA Sequencing and Analyses

Total RNA was isolated from three control and three *Rexo2* knockout mouse hearts using a miRNeasy Mini Kit (QIAGEN), incorporating an on-column RNase-free DNase digestion, according to manufacturer's instructions. RNA quantity, purity and integrity were verified using a Bioanalyzer. RNA sequencing was performed by the Cologne Genomics Centre (Cologne, Germany) on the Illumina HiSeq platform, according to the Illumina Tru-Seq protocol, using random hexamer primers for cDNA library generation and cytoplasmic rRNA depletion using the Ribo-Zero rRNA removal kit. Sequenced reads were aligned to the mouse genome reference sequence (mm10), masked for NUMTs regions, with bowtie2 v2.3.4.1 (Langmead and Salzberg, 2012),

with the–very-sensitive preset. Properly paired mitochondrial alignments were extracted, split by template strand and converted to full-length RNA fragment BED files, before coverage was calculated with BEDtools (Quinlan and Hall, 2010) genomecov (-d -scale [1e+06/total mapped reads]), normalized to the total number of fragments mapped to the mouse whole genome (reads per million; RPM), and converted to wig format for visualization. Gene-level counts for the nuclear genome were calculated with featureCounts (Liao et al., 2014) (-C –p –B –P -s 2) using the GENCODE vM20 annotation and a GENCODE-based mitochondrial annotation with contiguous *mt-Atp8/6* and *mt-Nd4l/4* intervals, and an approximate 7S RNA annotation (chrM:16035-16188). Count tables were collated in R v3.5.2 (R Development Core Team, 2010) and differential expression between conditions was analyzed with DESeq2 v1.22.2 (Love et al., 2014).

PARE and Analysis

PARE library preparation and sequencing was performed on RNA isolated from heart mitochondria from three control and three *Rexo2* knockout mouse hearts using a miRNeasy Mini Kit, as previously described (Mercer et al., 2011; Rackham and Filipovska, 2014) and sequencing was performed by Vertis Biotechnologie (Freising, Germany). The 5-bp adaptor sequence was trimmed and paired-end reads were merged with CLC Genomics Workbench (QIAGEN) if the read overlap exceeded 95% identity. Merged reads were aligned to the mouse genome (mm10) with Bowtie2, using the–very-sensitive preset parameters with a shortened seed length of 10 nt (Langmead and Salzberg, 2012), and strand-specific read coverage at the 5′ terminal position of aligned reads was calculated with BEDtools (Quinlan and Hall, 2010) genomecov (-d -scale [1e+06/total mapped reads]), normalized to the total number of fragments mapped to the mouse whole genome (reads per million; RPM), and converted to wig format for visualization. Relative changes were calculated as $\log_2$ fold changes of the mean normalized 5′ end coverage for three control (L/L) or knockout (L/L, cre) mice, plus a pseudocount of one. The genomic positions of the 5′ terminal nucleotides of all mapped reads were extracted using samtools, bedtools and awk. The corresponding strand-specific genomic sequences were extracted from the reference sequence and counted using bedtools and bash functions, and normalized to library size.

Purification of Proteins for *in vitro* Transcription

His-tagged human POLRMT, TFAM and TFB2M were expressed individually in *Spodoptera frugiperda* (Sf9) suspension cells infected with *Autographa californica* nuclear polyhedrosis virus stocks that were prepared using the BacPAK system (Clontech) according to manufacturer's instructions. Cells were collected 60-72 hours after infection and freeze-thawed in liquid nitrogen into a lysis buffer consisting of 20 mM Tris-HCl pH 8.0, 500 mM NaCl, 10 mM β-mercaptoethanol and 1 × proteinase inhibitors (1 mM PMSF, 2 mM pepstatin A, 0.6 mM leupeptin and 2 mM benzamidine in 100% ethanol). Proteins were purified by nickel and heparin affinity chromatography according to the method of Falkenberg et al. (2002). His-tagged human TEFM (residues 36-360) was expressed in KRX cells (Promega) and purified using sequential nickel affinity, heparin and gel filtration columns according to the method of Posse et al. (2015).

In vitro Transcription Reactions

Templates lacking a promoter sequence for *in vitro* transcription reactions consisted of pBluescript II SK(+), in either supercoiled form or linearized using BamHI and purified using a gel extraction kit (QIAGEN). Promoter-containing templates consisted of pUC18 containing the human mtDNA sequence region m. 1-477 (for LSP templates) or m. 499-742 (for HSP templates), inserted between BamHI and HindIII restriction sites. Where indicated, templates were linearized using BamHI (for LSP templates) or HindIII (for HSP templates) and purified using a PCR purification kit (QIAGEN). Standard *in vitro* transcription reactions (25 μl) consisted of 90 fmol DNA template, 500 fmol POLRMT, 500 fmol TFB2M, 5 pmol TFAM, 10 mM Tris-HCl (pH 8.0), 10 mM $MgCl_2$, 64 mM NaCl, 100 μg/ml BSA, 1 mM DTT, 4 U murine RNase inhibitor, 10 μM UTP, 0.02 μM [α-^{32}P] UTP (3000 Ci/mmol), and ATP, CTP and GTP as indicated in figure legends (either 20 μM each or 100 μM each). 1 pmol TEFM was also included where indicated. Reactions were allowed to proceed at 32°C for 30 minutes, before being stopped by the addition of 200 μl stop buffer (10 mM Tris-HCl (pH 8.0), 200 mM NaCl, 1 mM EDTA, 150 μg/ml proteinase K and 0.1 mg/ml glycogen). Reactions were incubated for a further 45 minutes at 42°C before being ethanol precipitated and resuspended in 10 μl loading buffer (98% formamide, 10 mM EDTA, 0.025% xylene cyanol and 0.025% bromophenol blue). Reactions were separated by 4% denaturing TBE-PAGE and imaged by autoradiography.

Primer Extension

In vitro transcription reactions were carried out as above, except that radiolabelled UTP was omitted and all NTPs were present at a final concentration of 100 μM. Following precipitation, transcription products were resuspended in 10 μl H_2O. This product (5 μl) was incubated with 1 pmol of end-labeled hLSP_PEx primer (labeled using T4 PNK according to manufacturer's instructions) at 65°C for 5 minutes then chilled on ice. Reverse transcription primer extension was carried out in first-strand buffer (50 mM Tris-HCl (pH 8.3), 75 mM KCl, 3 mM $MgCl_2$) with the addition of 10 mM DTT, 1 U RNase inhibitor, 0.5 mM each dNTP and 50 U SuperScript II (Thermo Scientific) at 42°C for 50 minutes, followed by inactivation at 70°C for 15 minutes. An equal volume of loading buffer was added and products were separated by 10% urea-PAGE on sequencing gels, and imaged by autoradiography.

QUANTIFICATION AND STATISTICAL ANALYSIS

Nuclease assays were quantified using MultiGauge V3.0 (Fujifilm) using images generated from a Fujifilm FLA-7000. Experiments using mouse samples were performed at least three times and results are representative of $n > 5$ independent biological replicates, unless indicated otherwise. All values are expressed as means ± SEM. Statistical significance between two groups was assessed by two-tailed unpaired Student's t test. Differences were considered statistically significant at a value of $p < 0.05$.

DATA AND CODE AVAILABILITY

Crystallography datasets are available at the RCSB Protein Data Bank with accession numbers PDB: 6RCI (REXO2), PDB: 6RCL (REXO2-pApA) and PDB: 6RCN (REXO2-dAdA).

The Gene Expression Omnibus (GEO) accession number for the data reported in this paper is GEO: GSE129707.

Original imaging data have been deposited in Mendeley Data and are available at https://doi.org/10.17632/ss68bdtccy.1